Electronic Supplementary Material (ESI) for ChemComm.

Supporting Information

Mesogenic discrete metallofoldamer for columnar liquid crystal

Shin-ichiro Kawano,[1] Kazutaka Narita,[1] Yuka Ikemoto,[2] Ako Sasaki,[1] and Kentaro Tanaka*[1]

[1] *Department of Chemistry, Graduate School of Science,*
Nagoya University, Furocho, Chikusa-ku, Nagoya 464-8602 (Japan)
[2] *Japan Synchrotron Radiation Research Institute/SPring-8,*
1-1-1 Kouto, Sayo-cho, Sayo-gun, Hyogo 679-5198, Japan

E-mail: kentaro@chem.nagoya-u.ac.jp

Contents

1. Experimental procedures

Synthetic procedures were carried out under dry nitrogen atmosphere, unless otherwise specified. All of the chemicals were purchased at the highest commercials quality available (Wako, Kanto, TCI, and Aldrich) and used without any further purification, unless otherwise stated. ^{1}H and ^{13}C NMR spectra were recorded on a JNM-ECS400 (400 MHz for ^{1}H; 100 MHz for ^{13}C), a JNM-ECS500 (500 MHz for ^{1}H; 125 MHz for ^{13}C), and JNM-ECA600 (600 MHz for ^{1}H; 150 MHz for ^{13}C) spectrometers. Tetramethylsilane (TMS) was used as an internal reference for ^{1}H and ^{13}C NMR measurements. Silica gel column chromatography was performed using Merck silica gel 60. GPC was performed using a JAI LC-9204 equipped with JAIGEL 2H-40/1H-40 or 2.5H-40/2.5H-40 columns. Elemental analyses were performed on a Yanaco MT-6 analyzer. Optical rotation was measured with a JASCO P-1010-GT polarimeter. ESI–TOF Mass spectroscopy was performed with a compact, Bruker. Matrix-assisted laser desorption ionization time-of-flight mass spectroscopy (MALDI-TOF-MS) was performed with an ultraflex III, Bruker Daltonics and dithranol or α-CHCA was used as the matrix. The absorption spectra were recorded with a Hitachi U-4100 spectrophotometer in $CHCl_3$ solutions at 20 ± 0.1 °C in 1.0 cm quartz cell. Circular dichroism spectra were recorded in in 1.0 cm quartz cell using a JASCO J-1500 CD spectrometer. Grazing incidence X-ray diffraction (GIXRD) analysis using CuK_α radiation was carried out for the samples placed on the glass plate on the temperature-controlled heating stage with various temperatures. The incidence angle in GIXRD was set to approximately 0.4°. The diffracted radiation was recorded by imaging plate with a sample-to-detector distance of 30 cm and exposure time of 5–30 min. The temperature of the sample was measured both with a thermocouple probe equipped in the X-ray stage and by an infrared ther- mometer (IT-550, HORIBA). For the powder X-ray diffraction experiment, the sample was loaded in a custom-made extrusion device. After heating the device to the desired temperature, the fiber was fabricated via extrusion at the liquid-crystalline phase. Typical extruded fiber dimensions are diameter 0.7 mm and length 0.5 to 11 mm. Infrared (IR) spectroscopy was carried out using JASCO FT/IR-6100 (KBr method or attenuated total reflection (ATR) method, Ge).

Microscopic IR spectroscopy was conducted at BL43IR beamline of SPring-8 (Hyogo, Japan) with a Fourier transform IR microscope system (VERTEX 70 and HYPERION 2000, Bruker) equipped with an MCT detector (No. 2021A1232, No. 2021B1127). The sample prepared on BaF_2 optical cell was installed into a temperature-controlled stage (LINKAM 10036L). IR spectra were recorded in transmission mode with a resolution of 4 cm^{-1} and 100–400 times integration with polarizer. Molecular force-field calculation was conducted with BIOVIA Materials Studio 2018 (18.1.0.2017).

2. Synthesis

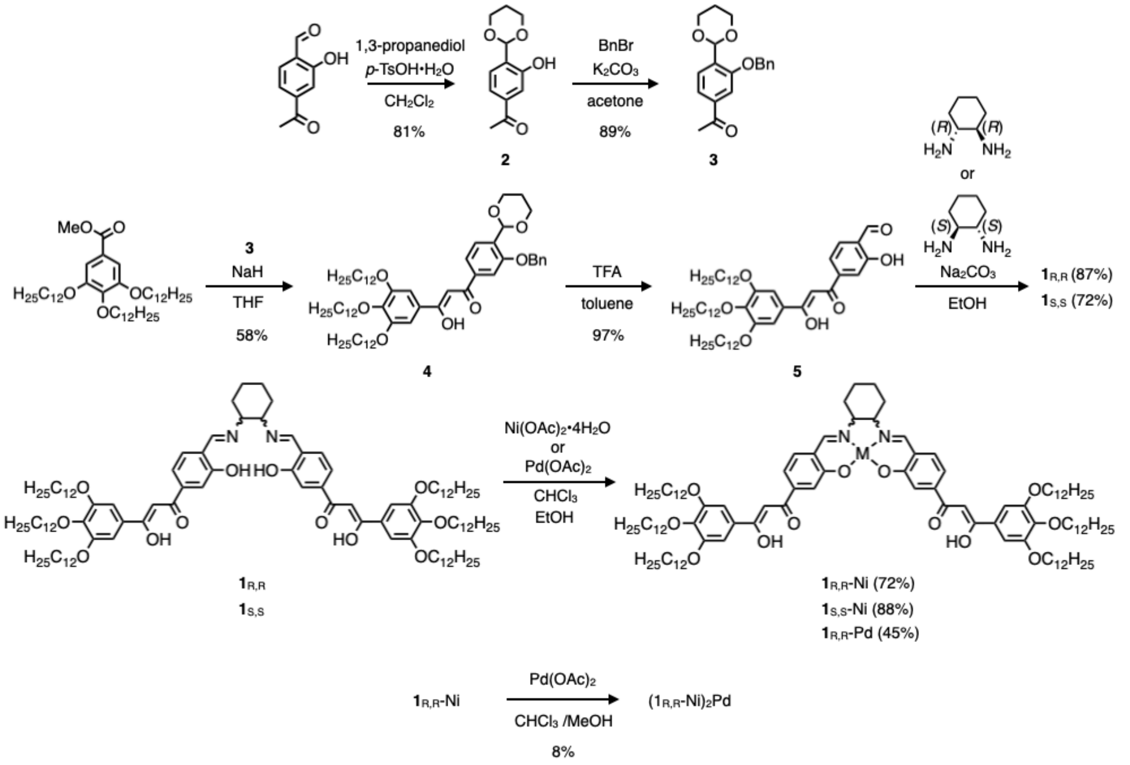

Scheme S1. Synthetic route of liquid-crystalline salen derivative.

Synthesis of 4-(1,3-dioxan-2-yl)-3-hydroxyacetophenone (**2**)

4-Acetylsalicylaldehyde[1] (2.00 g, 12.2 mmol) and *p*-TsOH•H_2O (68 mg, 0.36 mmol) were dissolved in dry CH_2Cl_2 (44 mL). Molecular sieve 3A (400 mg) and 1,3-propanediol (2.64 mL, 36.4 mmol) were added and the mixture was stirred for 25 h at room temperature, then the mixture was stirred for 14 h at 30 °C. A saturated solution of $NaHCO_3$ (50 mL) was added and the mixture was extracted with CH_2Cl_2 (50 mL × 3). The organic layer was dried over anhydrous Na_2SO_4, filtered and evaporated to obtain a crude product. The crude product was purified by column chromatography (SiO_2, 3.6 cm ϕ, 8.5 cm, hexane:AcOEt = 20:1) to obtain a colorless solid (2.19 g, 81%). ^{1}H NMR ($CDCl_3$/TMS, 400 MHz) δ: 8.00 (s, 1H), 7.45-7.43 (m, 2H), 7.26 (d, J = 8.7 Hz, 1H), 5.68 (s, 1H), 4.31 (dd, J = 12.0 Hz, 4.8 Hz, 2H), 4.02 (td, J = 12.5 Hz, 1.4 Hz, 2H), 2.38-2.21 (m, 1H), 1.54-1.51 (m, 1H). ^{13}C NMR ($CDCl_3$/TMS, 100 MHz) δ: 197.9, 155.5, 139.0, 128.1, 119.5, 117.2, 102.3, 67.6, 26.8, 25.7. ESI-TOF-MS: *m/z* = 245.0784 for calcd for $C_{12}H_{14}O_4Na$ ($[M+Na]^+$), found: 245.0774.

Synthesis of 3-(benzyloxy)-4-(1,3-dioxan-2-yl)-acetophenone (**3**)

Compound **2** (2.00 g, 9.00 mmol), K_2CO_3 (3.74 g, 27.0 mmol), and benzyl bromide (1.60 mL, 13.4 mmol) were suspended in dry acetone (20 mL). The mixture was stirred for 21.5 h. H_2O (100 mL) was added and the mixture was extracted with CH_2Cl_2 (100 mL × 3). The organic layer was dried over anhydrous Na_2SO_4, filtered and evaporated to obtain a crude product. The crude product was purified by reprecipitation from acetone and hexane to obtain the compound **3** as a yellow solid (2.49 g, 89%). ^{1}H NMR ($CDCl_3$/TMS, 400 MHz) δ: 7.72 (d, *J* = 7.8 Hz, 1H), 7.57-7.55 (m, 2H), 7.45 (d, *J* = 7.6 Hz, 2H), 7.41–7.37 (m, 2H), 7.32 (t, *J* = 7.6 Hz, 1H), 5.92 (s, 1H), 5.16 (s, 2H), 4.25 (dd, *J* = 11.2 Hz, 5.0 Hz, 2H), 3.99 (td, *J* = 12.7 Hz, 2.5 Hz, 2H), 2.31-2.19 (m, 1H), 1.43 (d, *J* = 14.0 Hz, 1H). ^{13}C NMR ($CDCl_3$/TMS, 100 MHz) δ: 197.9, 155.6, 138.6, 136.8, 132.4, 128.6, 128.0, 127.5, 127.3, 121.9, 111.2, 96.7, 70.5, 67.7, 26.8, 25.9. ESI-TOF-MS (pos.) : *m/z* = 335.1254 for calcd for $C_{19}H_{20}O_4Na$ ($[M+Na]^+$), found: 335.1267.

Synthesis of **4**

Compound **3** (1.50 g, 4.80 mmol), methyl 3,4,5-tris(dodecyloxy)benzoate (3.96 g, 5.74 mmol), and NaH (60%, 977 mg, 24.4 mmol) were suspended in dry THF (15 mL). The mixture was refluxed for 24 h. H_2O (150mL) and 1M HCl (20 mL) was added and the pH was adjusted to 7. The mixture was extracted with CH_2Cl_2 (100 mL × 6). The organic layer was dried over anhydrous Na_2SO_4, filtered and evaporated to obtain a crude product. The crude product was purified by recrystallization form 2-propanol and reprecipitation from $CHCl_3$ and 2-propanol to obtain the compound **4** as a pale yellow solid (2.63 g, 58%). The filtrate was further purified by column chromatography (SiO_2, 5.5 cm ϕ, 4 cm, hexane:AcOEt = 30:1) to obtain a target product (0.27 g, 6%, total 64%). ^{1}H NMR ($CDCl_3$/TMS, 400 MHz) δ: 16.9 (s, 1H), 7.73 (d, *J* = 8.3 Hz, 1H), 7.58-7.55 (m, 2H), 7.46 (d, *J* = 7.8 Hz, 2H), 7.42-7.01 (m, 2H), 7.34 (t, *J* = 7.8 Hz, 1H), 7.17 (s, 2H), 6.68 (s, 1H), 5.94 (s, 1H), 5.20 (s, 2H), 4.26 (dd, *J* = 11.7 Hz, 5.0 Hz, 2H), 4.06-3.97 (m, 8H), 2.30-2.21 (m, 1H), 1.86-1.71 (m, 6H), 1.55-1.26 (m, 48H, including H_2O), 0.87 (t, *J* = 7.3 Hz, 9H). ^{13}C NMR ($CDCl_3$/TMS, 100 MHz) δ: 186.4, 184.1, 156.1, 153.2, 142.7, 137.3, 136.9, 131.6, 130.5, 128.7, 128.0, 127.4, 127.3, 119.9, 110.9, 106.4, 96.8, 93.3, 73.7, 70.7, 69.6, 67.7, 32.0, 30.4, 29.8, 29.7, 29.5, 26.2, 25.9, 22.8, 14.2. ESI-TOF-MS: *m/z* = 969.7188 for calcd for $C_{62}H_{97}O_8$ ($[M+H]^+$), found: 969.7178.

Synthesis of **5**

Compound **4** (500 mg, 0.16 mmol) was dissolved in TFA (5.0 mL) and toluene (5.0 mL). The mixture was stirred at 85 °C for 1.5 h. A saturated solution of $NaHCO_3$ (150 mL) was added and the mixture was extracted with CH_2Cl_2 (150 mL × 2). The organic layer was dried over anhydrous Na_2SO_4, filtered and evaporated to obtain a crude product. The crude product was purified by reprecipitation from $CHCl_3$ and MeOH to obtain a yellow solid (411 mg, 97%). ^{1}H NMR ($CDCl_3$/TMS, 400 MHz) δ: 16.7 (s, 1H), 11.0 (s, 1H), 9.97 (s, 1H), 7.68 (d, J = 8.2 Hz, 1H), 7.59 (d, J = 8.2 Hz, 1H), 7.54 (s, 1H), 7.19 (s, 2H), 6.74 (s, 1H), 4.05 (t, J = 6.4 Hz, 6H), 1.87-1.71 (m, 6H), 1.54-1.45 (m, 6H, including H_2O), 1.25–1.20 (m, 42H), 0.87 (t, J = 6.9 Hz, 6H). ^{13}C NMR ($CDCl_3$/TMS, 100 MHz) δ: 196.3, 188.5, 180.5, 161.5, 153.3, 143.0, 134.0, 130.3, 122.4, 118.2, 116.2, 106.4, 94.2, 73.7, 69.5, 32.0, 30.4, 29.8, 29.7, 29.5, 26.2, 22.8, 14.2. ESI-TOF-MS: *m/z* =821.6278 for calcd for $C_{52}H_{85}O_7$ ($[M+H]^+$), found: 821.6290.

Synthesis of $\mathbf{1}_{R,R}$

Compound **5** (100 mg, 0.122 mmol), (1*R*,2*R*)-(-)-1,2-cyclohexanediamine (11.4 mg, 0.0609 mmol) and Na_2CO_3 (64 mg, 0.604 mmol) were suspended in dry EtOH (1.0 mL). The mixture was refluxed for 1 h. The mixture was decantated and washed with MeOH, the residue was dissolved in $CHCl_3$ and filtered. The filtrate was evaporated to obtain a crude product. The crude product was purified by GPC (JAIGEL 2H-1H, $CHCl_3$) to obtain $\mathbf{1}_{R,R}$ as an orange oil (91 mg, 87%). ^{1}H NMR ($CDCl_3$/TMS, 400 MHz) δ: 16.8 (s, 2H), 13.3 (brs, 2H), 8.33 (s, 2H), 7.46 (d, J = 1.2 Hz, 2H), 7.40 (dd, J = 8.0 Hz, J = 1.6 Hz, 2H), 7.26 (d, J = 8.4 Hz, 2H, including $CHCl_3$), 7.17 (s, 4H), 6.69 (s, 2H), 4.04 (t, J = 6.4 Hz, 12H), 3.41-3.39 (m, 2H), 2.15-1.92 (m, 4H), 1.86-1.71 (m, 14H), 1.57-1.47 (m, 12H), 1.40-1.20 (m, 96H), 0.88 (t, J = 6.4 Hz, 18H). ^{13}C NMR ($CDCl_3$/TMS, 100 MHz) δ: 187.5, 182.3, 164.3, 160.9, 153.2, 142.7, 138.7, 131.7, 130.6, 121.2, 117.3, 115.4, 106.2, 93.5, 73.7, 72.9, 69.5, 33.0, 32.0, 30.4, 29.8, 29.7, 29.5, 26.2, 24.2, 22.8, 14.2. ESI-TOF-MS: *m/z* = 1742.3272 for calcd for $C_{110}H_{178}N_2O_{12}Na$ ($[M+Na]^+$), found: 1742.3297.

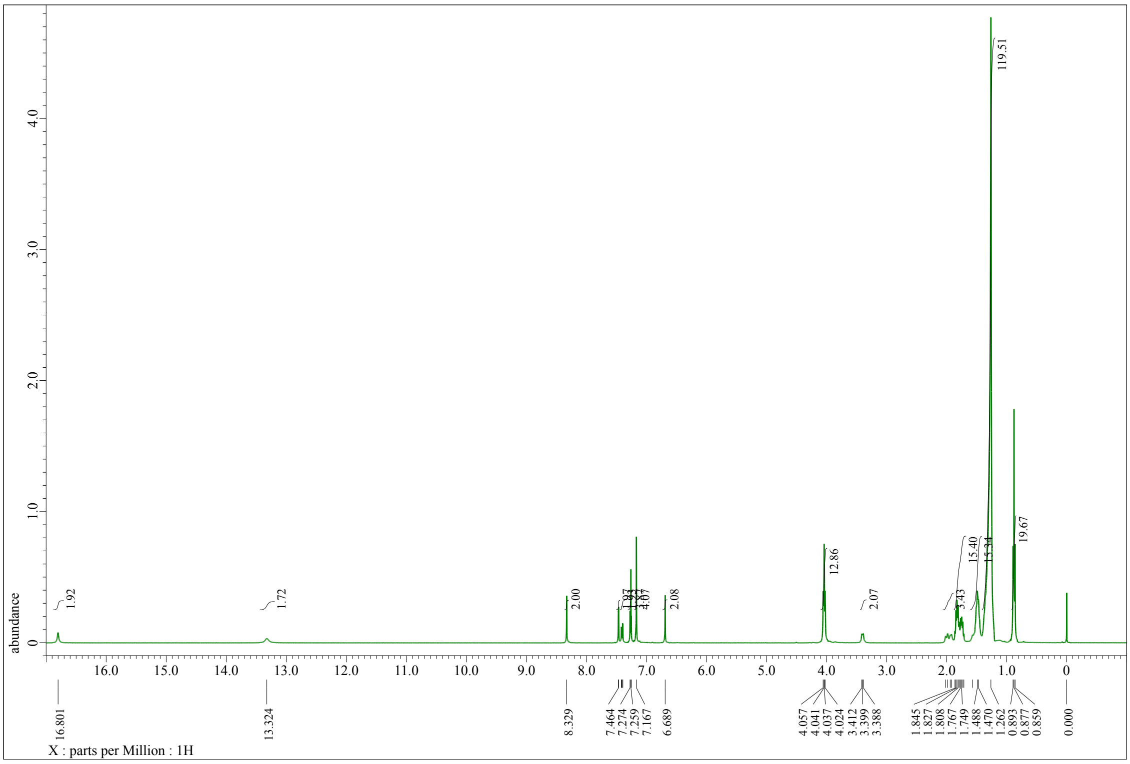
abundance
0
1.0
2.0
3.0
4.0
16.0
15.0
14.0
13.0
12.0
11.0
10.0
9.0
8.0
7.0
6.0
5.0
4.0
3.0
2.0
1.0
0
X : parts per Million : 1H
1.92
1.72
2.00
1.87
1.83
4.07
2.08
12.86
2.07
3.43
15.40
15.34
119.51
19.67
16.801
13.324
8.329
7.464
7.274
7.259
7.167
6.689
4.057
4.041
4.037
4.024
3.412
3.399
3.388
1.845
1.827
1.808
1.767
1.749
1.488
1.470
1.262
0.893
0.877
0.859
0.000

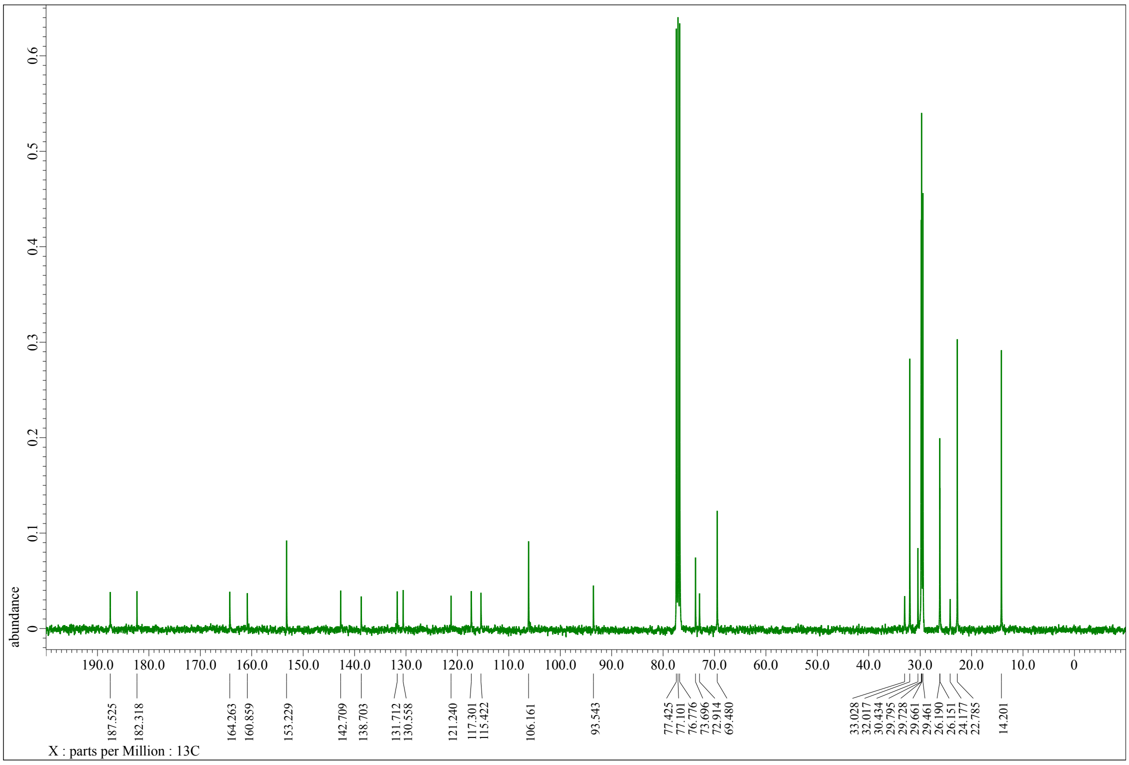
abundance
0
0.1
0.2
0.3
0.4
0.5
0.6
190.0
180.0
170.0
160.0
150.0
140.0
130.0
120.0
110.0
100.0
90.0
80.0
70.0
60.0
50.0
40.0
30.0
20.0
10.0
0
X : parts per Million : 13C
187.525
182.318
164.263
160.859
153.229
142.709
138.703
131.712
130.558
121.240
117.301
115.422
106.161
93.543
77.425
77.101
76.776
73.696
72.914
69.480
33.028
32.017
30.434
29.795
29.728
29.661
29.461
26.190
26.151
24.177
22.785
14.201

Synthesis of **1**$_{S,S}$

1$_{S,S}$ was obtained as an orange oil with the similar procedure to that of the enantiomer (49 mg, 72%). ^{1}H NMR (CDCl$_3$/TMS, 400 MHz) δ: 16.8 (s, 2H), 13.4 (brs, 2H), 8.33 (s, 2H), 7.47 (d, *J* = 1.2 Hz, 2H), 7.40 (d, *J* = 8.4 Hz, *J* = 1.6 Hz, 2H), 7.29-7.28 (m, 2H, including CHCl$_3$), 7.17 (s, 4H), 6.69 (s, 2H), 4.06–4.02 (m, 12H), 3.42-3.40 (m, 2H), 2.02-1.92 (m, 4H), 1.86-1.71 (m, 14H), 1.56-1.20 (m, 110H), 0.88 (t, *J* = 6.8 Hz, 18H). ^{13}C NMR (CDCl$_3$/TMS, 100 MHz) δ: 187.5, 182.3, 164.3, 160.9, 153.2, 142.7, 138.7, 131.7, 130.6, 121.2, 117.3, 115.4, 106.2, 93.5, 73.7, 72.9, 69.5, 33.0, 32.0, 30.4, 29.8, 29.7, 29.7, 29.5, 26.2, 24.2, 22.8, 14.2. ESI-TOF-MS: *m/z* = 1742.3272 for calcd for $C_{110}H_{178}N_2O_{12}Na$ ([M+Na]$^+$), found: 1742.3250.

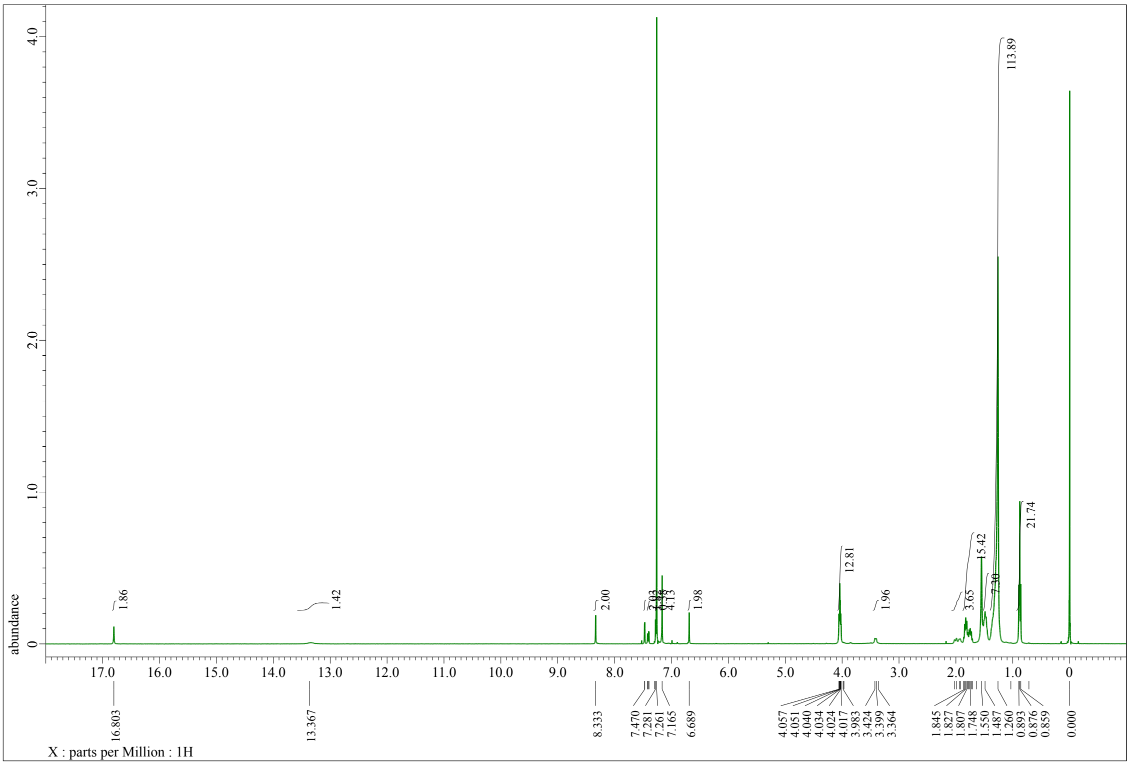
abundance
0
1.0
2.0
3.0
4.0
1.86
1.42
2.00
2.03
4.13
1.98
12.81
1.96
3.65
15.42
7.30
13.89
21.74
17.0
16.0
15.0
14.0
13.0
12.0
11.0
10.0
9.0
8.0
7.0
6.0
5.0
4.0
3.0
2.0
1.0
0
16.803
13.367
8.333
7.470
7.281
7.261
7.165
6.689
4.057
4.051
4.040
4.034
4.024
4.017
3.983
3.424
3.399
3.364
1.845
1.827
1.807
1.748
1.550
1.487
1.260
0.893
0.876
0.859
0.000
X : parts per Million : 1H

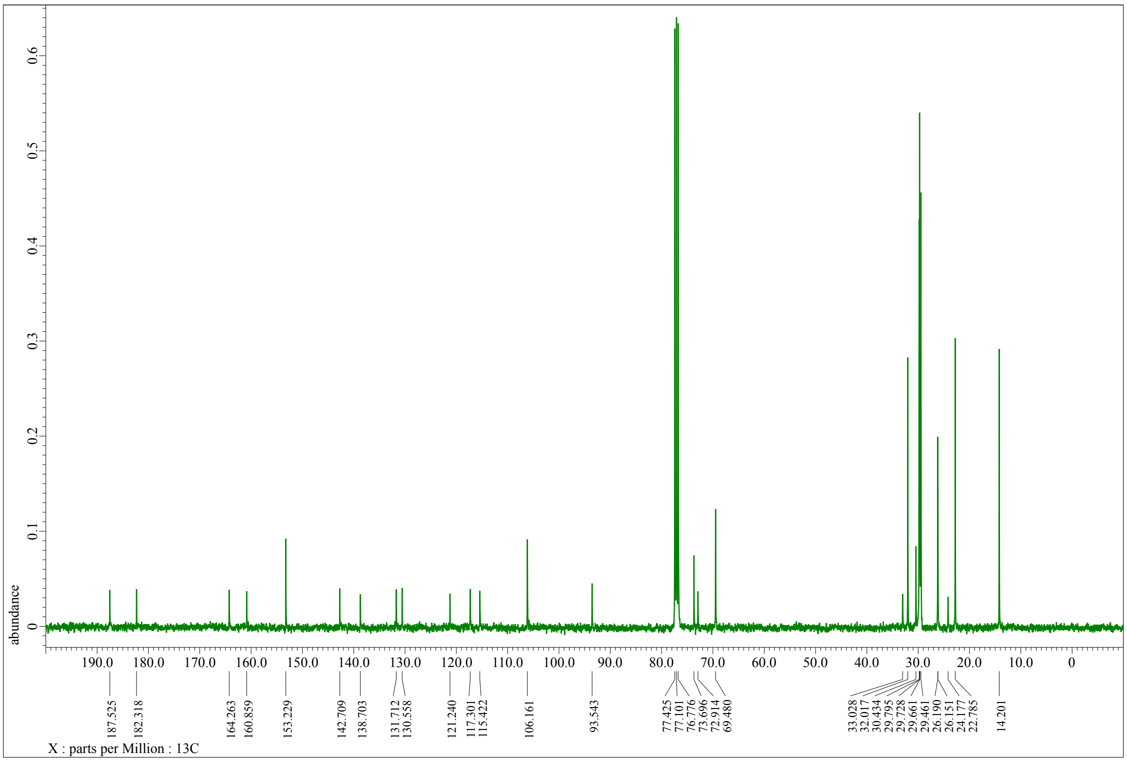
abundance
0
0.1
0.2
0.3
0.4
0.5
0.6
190.0
180.0
170.0
160.0
150.0
140.0
130.0
120.0
110.0
100.0
90.0
80.0
70.0
60.0
50.0
40.0
30.0
20.0
10.0
0
187.525
182.318
164.263
160.859
153.229
142.709
138.703
131.712
130.558
121.240
117.301
115.422
106.161
93.543
77.425
77.101
76.776
73.696
72.914
69.480
33.028
32.017
30.434
29.795
29.728
29.661
29.461
26.190
26.151
24.177
22.785
14.201
X : parts per Million : 13C

Synthesis of **1**$_{R,R}$-Pd

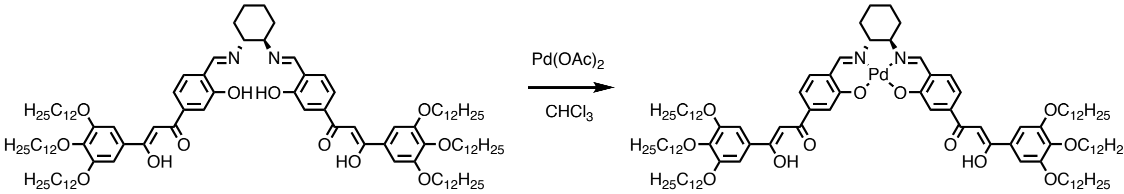

This reaction was performed under N$_2$ atmosphere and all reaction vessels were dried up. Compound **1**$_{R,R}$ (100 mg, 58.1 μmol), Pd(OAc)$_2$ (19.7 mg, 87.7 μmol) were suspended in dry CHCl$_3$ (6 mL). The mixture was heated for 36 h at 40 °C. The reaction mixture was filtered with Celite® and a precipitate was washed with CH$_2$Cl$_2$. The filtrate was evaporated to obtain a crude product (125 mg, 118%). The crude product was purified by GPC (JAIGEL 2.5H-3H, CHCl$_3$) and GPC (JAIGEL 2H-1H, CHCl$_3$) to obtain **1**$_{R,R}$-Pd as an orange solid (48 mg, 45%). $[\alpha]^{20}_{D}$ –256.7° (*c* 0.5, CHCl$_3$). ^{1}H NMR (CDCl$_3$/TMS, 400 MHz) δ: 16.8 (s, 2H), 7.66 (s, 2H), 7.42 (s, 2H), 7.22 (s, 6H, including CHCl$_3$), 7.03-6.98 (m, 4H), 6.74 (s, 2H), 4.10-4.04 (m, 14H), 3.69 (s, 2H), 2.45 (s, 2H), 1.96 (s, 2H), 1.88-1.73 (m, 14H), 1.51-1.25 (m, 149H), 0.86 (t, *J* = 6.4 Hz, 21H). ^{13}C NMR (CDCl$_3$/TMS, 100 MHz) δ: 187.3, 183.2, 164.8, 155.0, 153.3, 142.6, 140.8, 135.3, 130.6, 123.4, 120.3, 112.8, 105.9, 93.7, 73.7, 72.5, 69.5, 32.0, 30.5, 29.9, 29.8, 29.6, 29.5, 28.6, 26.3, 26.2, 24.6, 22.8, 14.2. ESI-TOF-MS: *m/z* = 1844.2161 for calcd for $C_{110}H_{176}N_2O_{12}PdNa$ ([M+Na]$^+$), found : 1844.2197. Anal. Calcd for $C_{110}H_{176}N_2O_{12}Pd$: C, 72.39; H, 9.72; N, 1.53. found: C, 72.00; H, 10.10; N, 1.43.

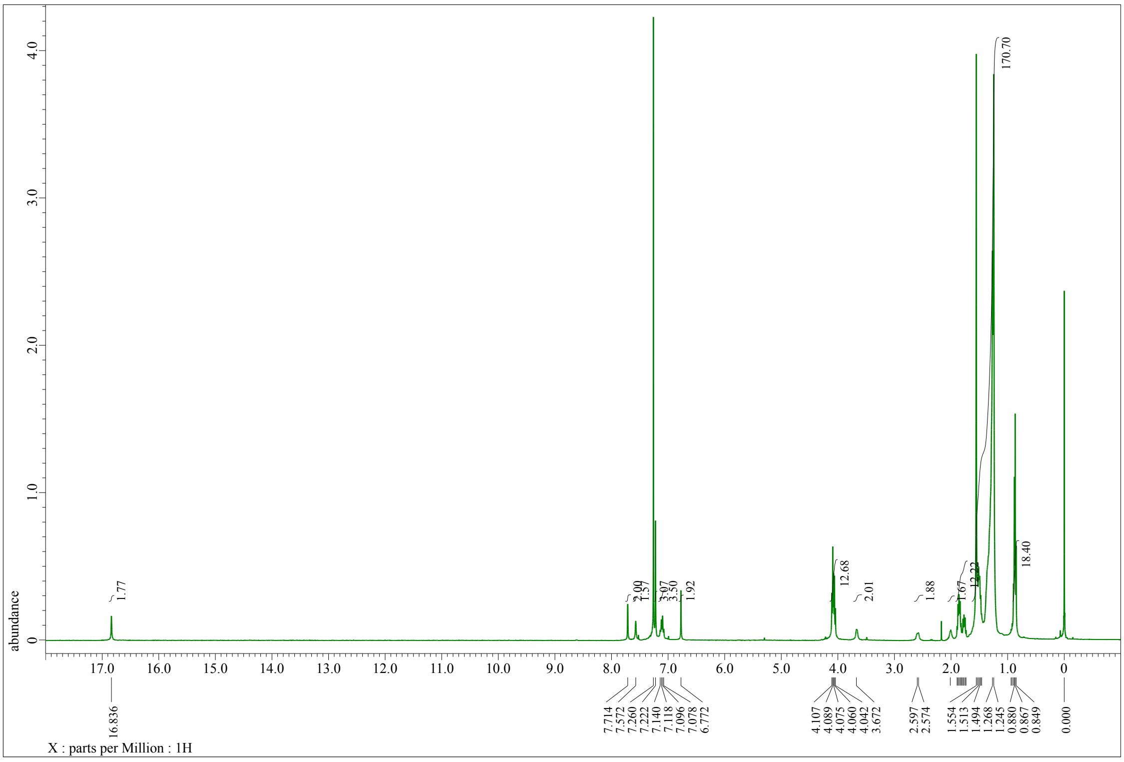
abundance
0
1.0
2.0
3.0
4.0
1.77
2.00
1.57
3.07
3.50
1.92
12.68
2.01
1.88
1.67
12.22
170.70
18.40
17.0
16.0
15.0
14.0
13.0
12.0
11.0
10.0
9.0
8.0
7.0
6.0
5.0
4.0
3.0
2.0
1.0
0
16.836
7.714
7.572
7.260
7.222
7.140
7.118
7.096
7.078
6.772
4.107
4.089
4.075
4.060
4.042
3.672
2.597
2.574
1.554
1.513
1.494
1.268
1.245
0.880
0.867
0.849
0.000
X : parts per Million : 1H

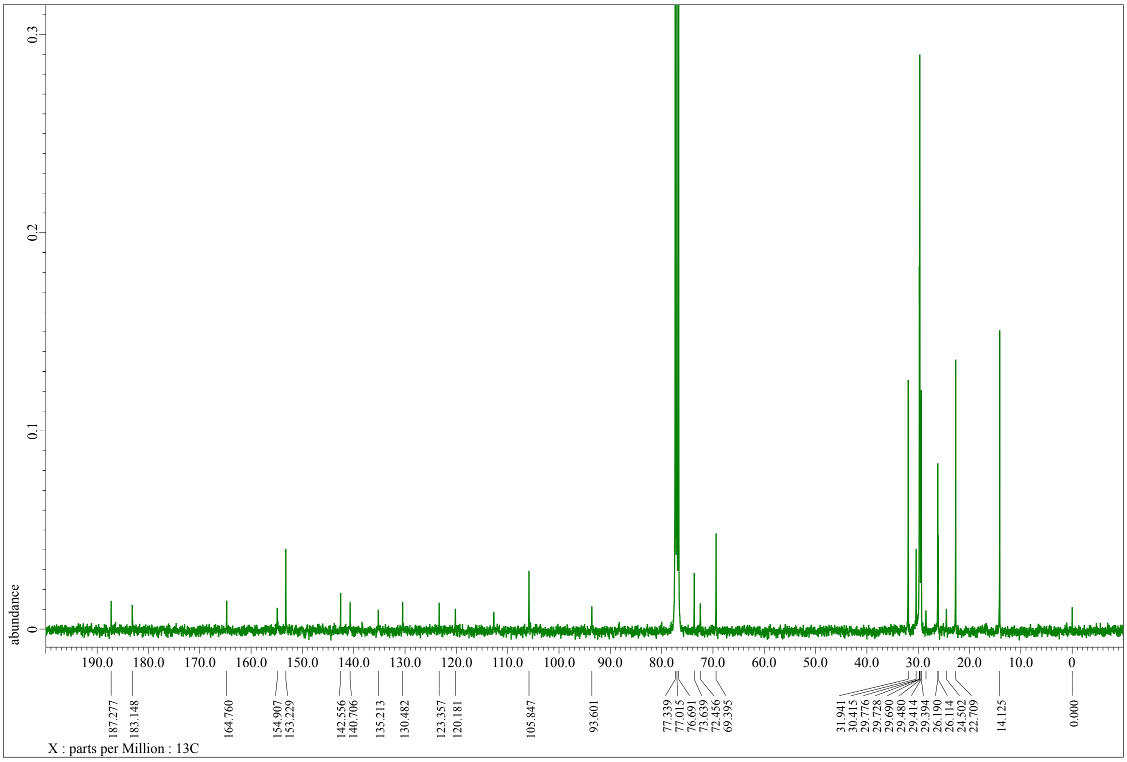
abundance
0
0.1
0.2
0.3
190.0
180.0
170.0
160.0
150.0
140.0
130.0
120.0
110.0
100.0
90.0
80.0
70.0
60.0
50.0
40.0
30.0
20.0
10.0
0
187.277
183.148
164.760
154.907
153.229
142.556
140.706
135.213
130.482
123.357
120.181
105.847
93.601
77.339
77.015
76.691
73.639
72.456
69.395
31.941
30.415
29.776
29.728
29.690
29.480
29.414
29.394
26.190
26.114
24.502
22.709
14.125
0.000
X : parts per Million : 13C

Synthesis of **1**$_{R,R}$-Ni

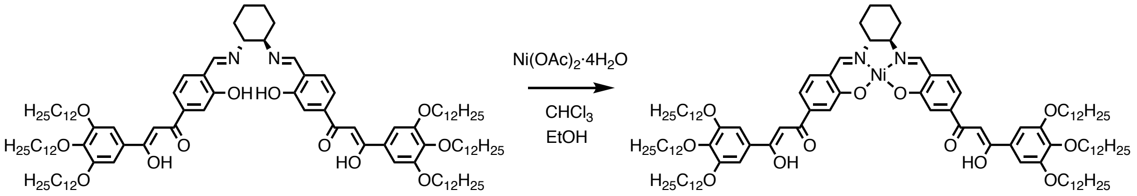

Compound **1**$_{R,R}$ (250 mg, 0.145 mmol) and Ni(OAc)$_2$·4H$_2$O (36 mg, 0.145 mmol) were dissolved in dry CHCl$_3$ (9 mL) and dry EtOH (9 mL). The mixture was refluxed for 1 h. The reaction mixture was filtered with cellulose powder (200~300 mesh). The filtrate was evaporated to obtain a crude product (265 mg, 103%). The crude product was purified by GPC (JAIGEL 3H-2.5H, CHCl$_3$) and reprecipitated from EtOH and CH$_2$Cl$_2$ to obtain **1**$_{R,R}$-Ni as a red solid (186 mg, 72%). $[\alpha]^{21}_{\mathrm{D}}$ –527.7° (*c* 0.2, CHCl$_3$). ^{1}H NMR (CDCl$_3$/TMS, 323K, 400 MHz) δ: 16.7 (s, 2H), 7.60 (s, 2H), 7.37 (s, 2H), 7.21 (s, 4H), 7.10 (s, 4H), 6.73 (s, 2H), 4.09-4.04 (m, 12H), 3.25-3.20 (m, 2H), 2.48-2.40 (m, 2H), 1.98-1.94 (m, 2H), 1.87-1.73 (m, 14H), 1.54-1.20 (m, 110H), 0.89-0.85 (m, 18H). ^{13}C NMR (CDCl$_3$/TMS, 100 MHz) δ: 187.1, 183.3, 163.9, 157.2, 153.2, 142.4, 139.9, 133.1, 130.4, 122.5 120.0, 113.0, 105.7, 93.5, 73.6, 70.3, 69.3, 31.9, 30.4, 29.8, 29.8, 29.7, 29.5, 29.4, 28.7, 26.2, 26.1, 24.3, 22.7, 14.1. ESI-TOF MS : *m/z* = 1798.2469 for calcd for $C_{110}H_{176}N_2O_{12}NiNa$ ([M+Na]$^+$), found : 1798.2441. Anal. Calcd for $C_{110}H_{176}N_2O_{12}Ni$: C, 74.34; H, 9.98; N, 1.58. found: C, 74.10; H, 10.17; N, 1.63.

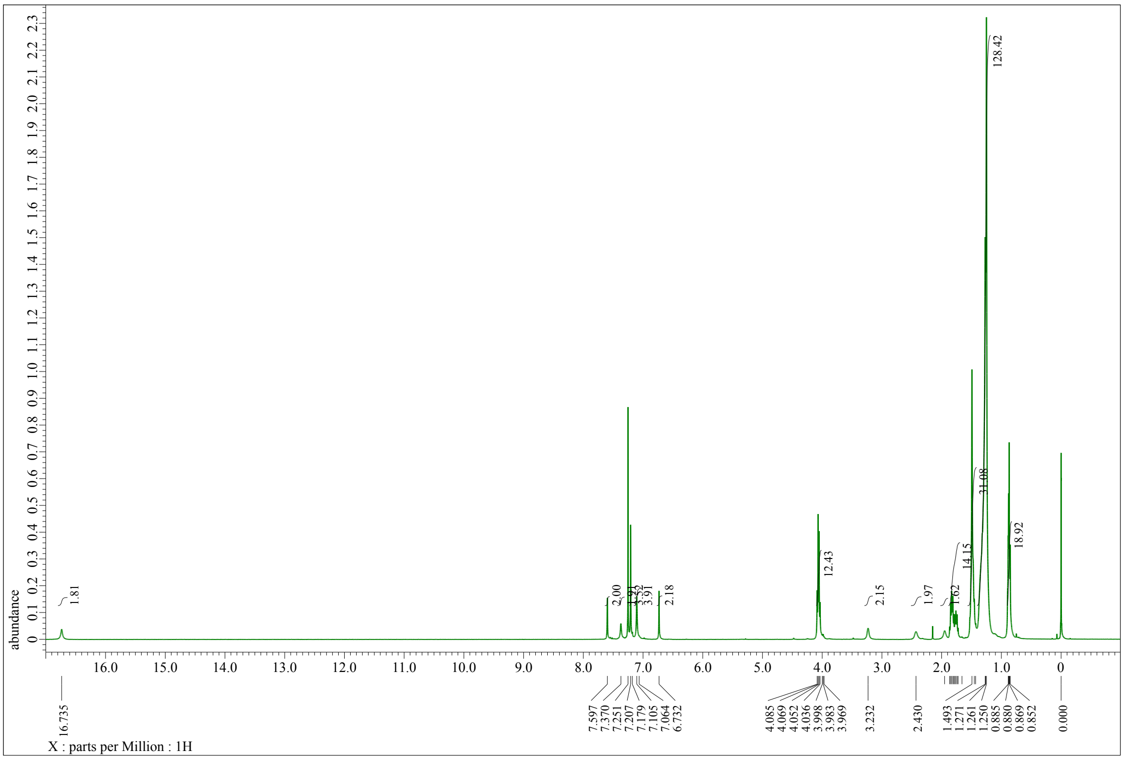
abundance
X : parts per Million : 1H
16.735
7.597
7.370
7.251
7.207
7.179
7.105
7.064
6.732
4.085
4.069
4.052
4.036
3.998
3.983
3.969
3.232
2.430
1.493
1.271
1.261
1.250
0.885
0.880
0.869
0.852
0.000
1.81
2.00
2.01
4.22
3.52
3.91
2.18
12.43
2.15
1.97
1.62
14.15
31.08
128.42
18.92

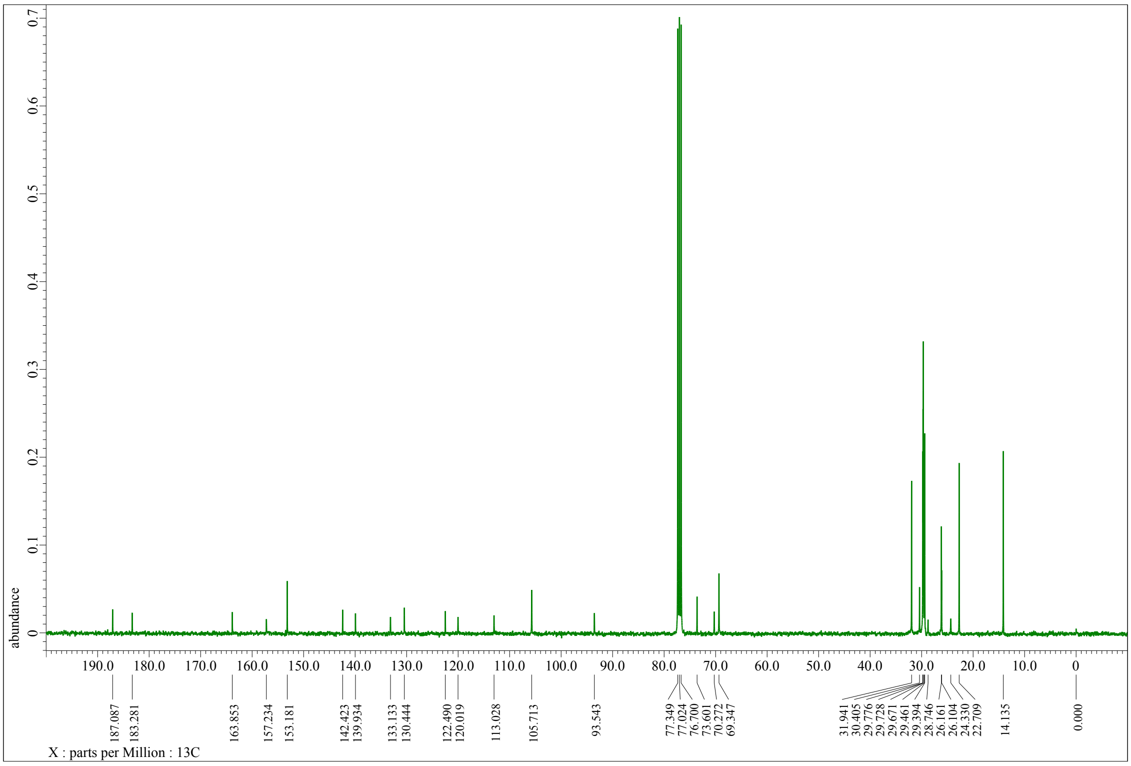
abundance
X : parts per Million : 13C
187.087
183.281
163.853
157.234
153.181
142.423
139.934
133.133
130.444
122.490
120.019
113.028
105.713
93.543
77.349
77.024
76.700
73.601
70.272
69.347
31.941
30.405
29.776
29.728
29.671
29.461
29.394
28.746
26.161
26.104
24.330
22.709
14.135
0.000

Synthesis of $\mathbf{1}_{S,S}$-Ni

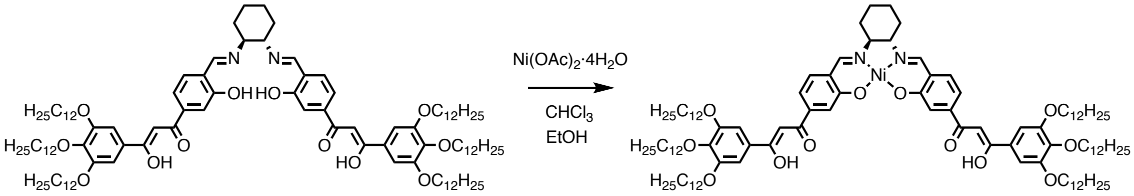

$\mathbf{1}_{S,S}$-Ni was prepared as a red solid with the similar method to $\mathbf{1}_{R,R}$-Ni (87 mg, 88%). $[\alpha]^{21}_{D}$ 537.4° (*c* 0.2, $CHCl_3$). ^1H NMR ($CDCl_3$/TMS, 323K, 400 MHz) δ: 16.8 (s, 2H), 7.63 (s, 2H), 7.49 (s, 2H), 7.22 (d, *J* = 8.8 Hz, 2H), 7.20 (s, 4H), 7.16 (d, *J* = 8.4 Hz, 2H), 6.76 (s, 2H), 4.08-4.03 (m, 12H), 3.21-3.19 (m, 2H), 2.51-2.49 (m, 2H), 2.00–1.99 (m, 2H), 1.87-1.72 (m, 12H), 1.52-1.23 (m, 112H), 0.89-0.85 (m, 18H). ^{13}C NMR ($CDCl_3$/TMS, 100 MHz) δ: 187.1, 183.3, 163.9, 157.2, 153.2, 142.4, 139.9, 133.1, 130.4, 122.5 120.0, 113.0, 105.7, 93.5, 73.6, 70.3, 69.3, 31.9, 30.4, 29.8, 29.8, 29.7, 29.5, 29.4, 28.7, 26.2, 26.1, 24.3, 22.7, 14.1. ESI-TOF MS : *m/z* = 1798.2469 for calcd for $C_{110}H_{176}N_2O_{12}NiNa$ ($[M+Na]^+$), found: 1798.2452. Anal. Calcd for $C_{110}H_{176}N_2O_{12}Ni$: C, 74.34; H, 9.98; N, 1.58. found: C, 74.71; H, 10.11; N, 1.76.

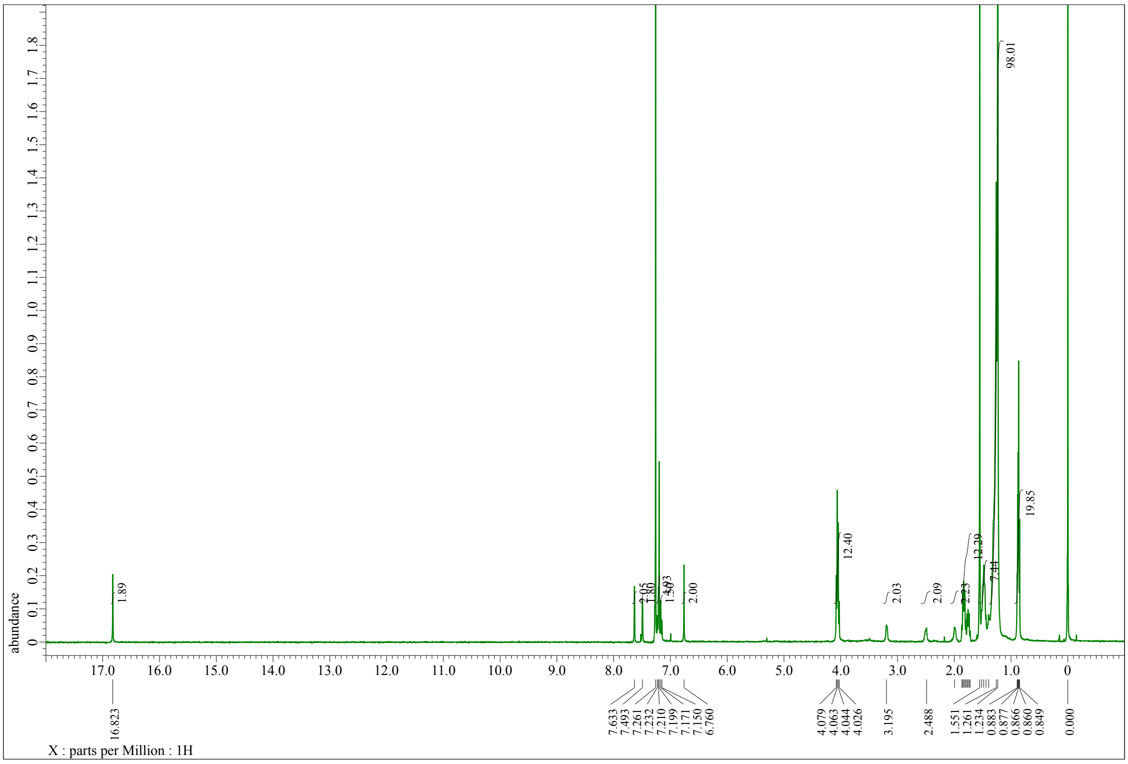
abundance
0
0.1
0.2
0.3
0.4
0.5
0.6
0.7
0.8
0.9
1.0
1.1
1.2
1.3
1.4
1.5
1.6
1.7
1.8
1.89
2.05
1.80
4.03
1.50
2.00
12.40
2.03
2.09
2.23
12.29
7.44
98.01
19.85
17.0
16.0
15.0
14.0
13.0
12.0
11.0
10.0
9.0
8.0
7.0
6.0
5.0
4.0
3.0
2.0
1.0
0
16.823
7.633
7.493
7.261
7.232
7.210
7.199
7.171
7.150
6.760
4.079
4.063
4.044
4.026
3.195
2.488
1.551
1.261
1.234
0.883
0.877
0.866
0.860
0.849
0.000
X : parts per Million : 1H

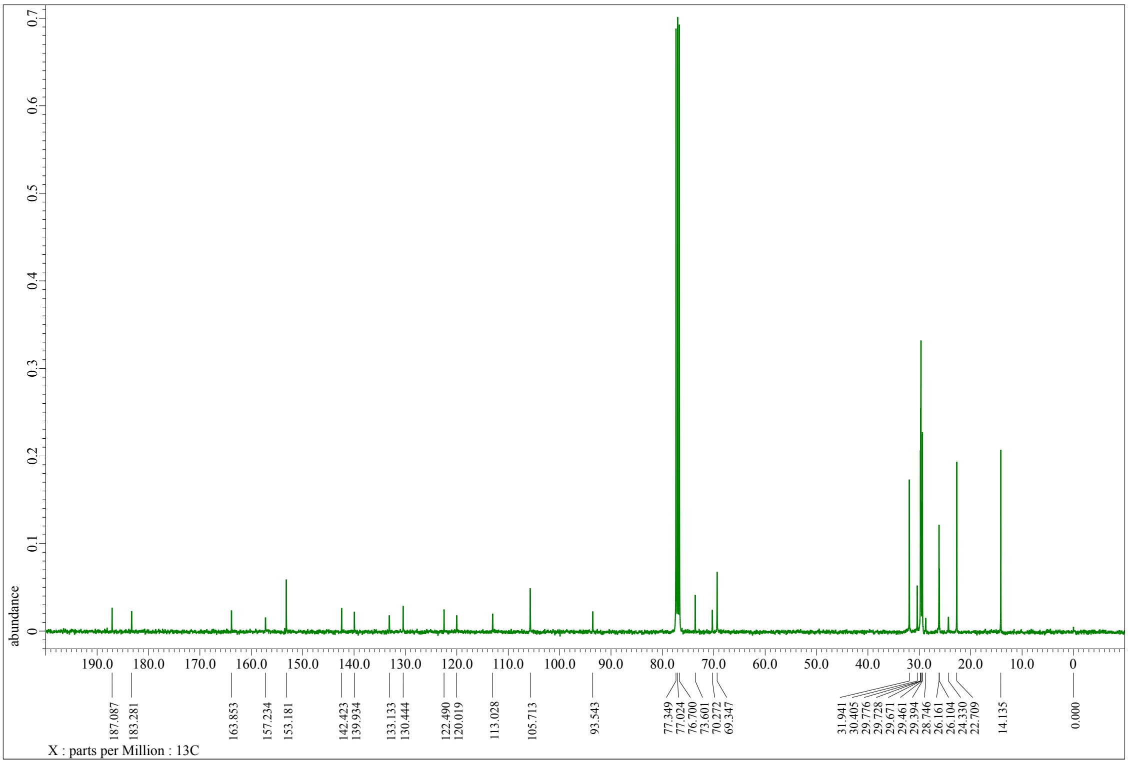
abundance
0
0.1
0.2
0.3
0.4
0.5
0.6
0.7
190.0
180.0
170.0
160.0
150.0
140.0
130.0
120.0
110.0
100.0
90.0
80.0
70.0
60.0
50.0
40.0
30.0
20.0
10.0
0
187.087
183.281
163.853
157.234
153.181
142.423
139.934
133.133
130.444
122.490
120.019
113.028
105.713
93.543
77.349
77.024
76.700
73.601
70.272
69.347
31.941
30.405
29.776
29.728
29.671
29.461
29.394
28.746
26.161
26.104
24.330
22.709
14.135
0.000
X : parts per Million : 13C

Synthesis of $(\mathbf{1}_{R,R}\text{-Ni})_2\text{Pd}$

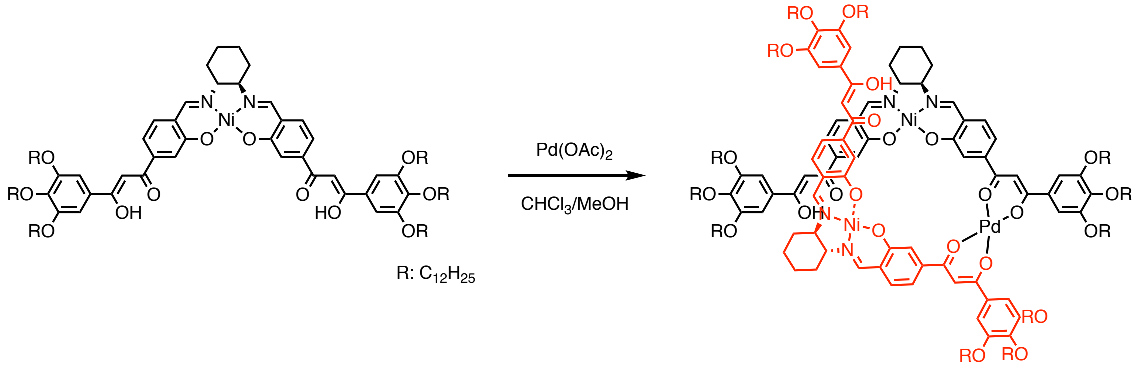

$\mathbf{1}_{R,R}$-Ni (100 mg, 56 μmol) and $Pd(OAc)_2$ (6.3 mg, 28 μmol) were dissolved in dry $CHCl_3$ (22 mL) and dry MeOH (4.4 mL). The mixture was stirred for 12.5 h at 50 °C. The reaction mixture was evaporated to obtain a crude product (100 mg, 98%). The crude product was purified by SCC (3.0 cm ϕ, 16 cm, $CHCl_3$:Et_2O = 100:1), SCC (3 cm *ϕ*, 19 cm, $CHCl_3$:Et_2O = 50:1~10:1), and GPC (JAIGEL 3H-2.5H, $CHCl_3$) ×3 to obtain $(\mathbf{1}_{R,R}\text{-Ni})_2$Pd as a red solid (8.1 mg, 8%). $[\alpha]^{20}_{D}$ –167.0° (*c* 0.2, $CHCl_3$). ^{1}H NMR (THF-d_8:CD_3CN = 5:1/TMS, 323 K 600 MHz) δ: 17.4 (s, 2H), 7.72 (s, 4H), 7.54 (s, 2H), 7.51 (s, 2H), 7.47 (s, 2H), 7.28-7.23 (m, 8H), 7.19 (d, *J* = 8.4 Hz, 2H), 7.12 (d, *J* = 7.8 Hz, 2H), 6.94 (d, *J* = 8.4 Hz, 2H), 6.84 (s, 2H), 6.75 (d, *J* = 7.8 Hz, 2H), 4.04 (t, *J* = 6.0 Hz, 6H), 4.01-3.97 (m, 10H), 3.92-3.84 (m, 8H), 2.39 (brs, 2H), 2.26 (brs, 2H), 2.08-2.06 (m, 2H), 1.81–1.72 (m, 12H), 1.57-1.49 (m, 24H), 1.42-1.11 (m, 204H), 0.87-0.79 (m, 36H). ^{13}C NMR ($CDCl_3$/TMS, 125 MHz) *δ*: 185.5, 184.5, 181.3, 180.2, 164.1, 163.7, 156.8, 156.6, 153.3, 152.8, 141.8, 141.7, 140.4, 138.6, 132.7, 132.6, 132.2, 130.6, 130.3, 122.5, 122.0, 121.0, 113.4, 112.6, 106.8, 105.2, 95.7, 93.4, 73.5, 70.3, 70.0, 69.5, 69.4, 32.1, 30.4, 30.4, 29.9, 29.9, 29.8, 29.7, 29.6, 29.6, 29.4, 28.5, 28.4, 26.3, 26.2, 26.2, 26.1, 24.4, 22.7, 14.1. ESI-TOF MS : *m/z* = 3677.39 for calcd for $C_{220}H_{350}N_4Ni_2O_{24}PdNa$ ($[M+Na]^+$), found : 3677.35. Anal. Calcd for $C_{220}H_{350}N_4Ni_2O_{24}Pd$: C, 72.22; H, 9.64; N, 1.53. found: C, 72.02; H, 9.93; N, 1.56.

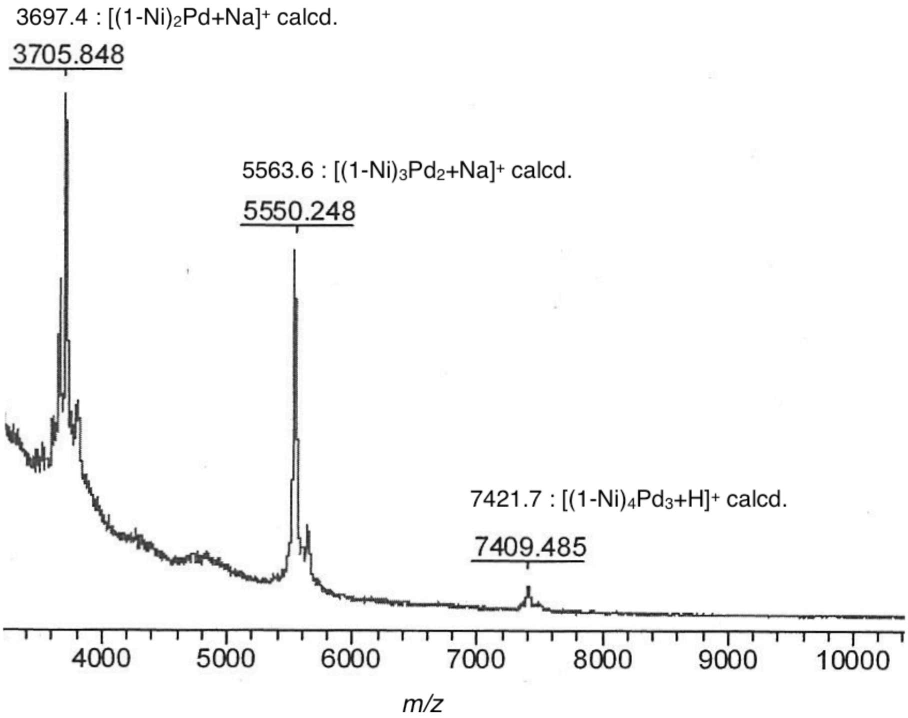

Figure S1. MALDI-TOF MS spectrum of the reaction product of the helical oligomer (α-CHCA, LP-Mode)

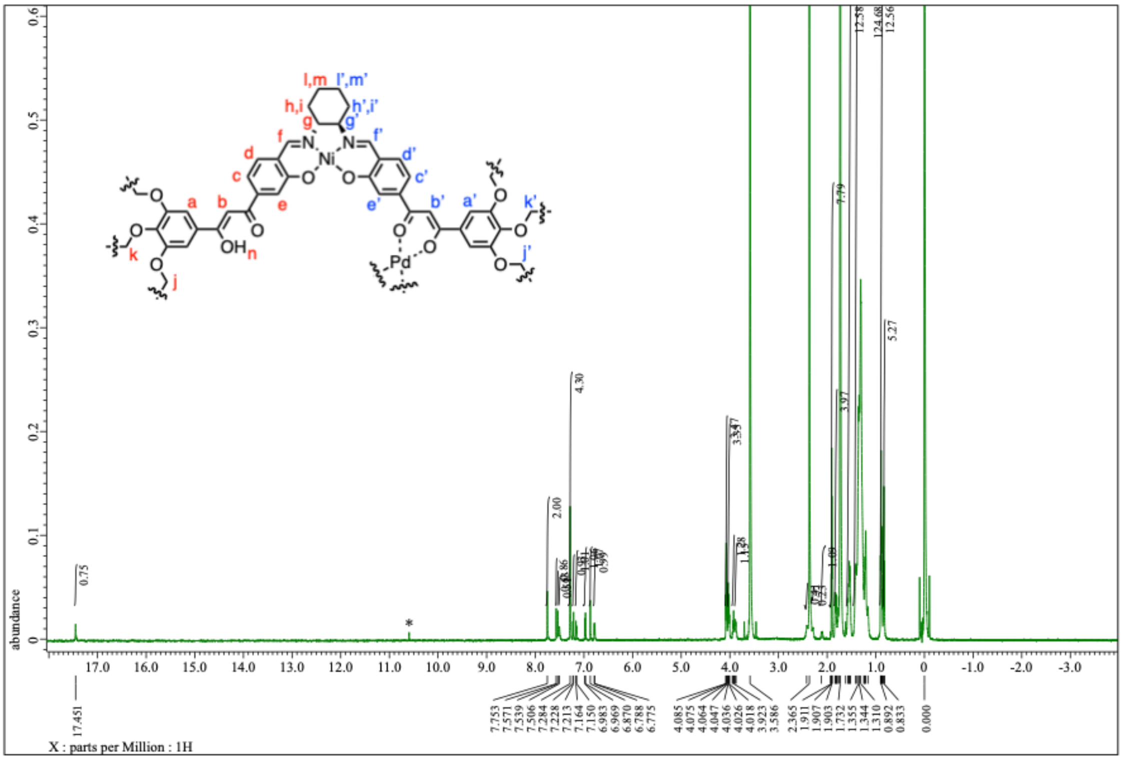

Figure S2. ^{1}H NMR spectrum of ($\mathbf{1}_{R,R}$-Ni)$_2$Pd (600 MHz,THF-d_8:CD_3CN = 5:1, TMS, 323 K)

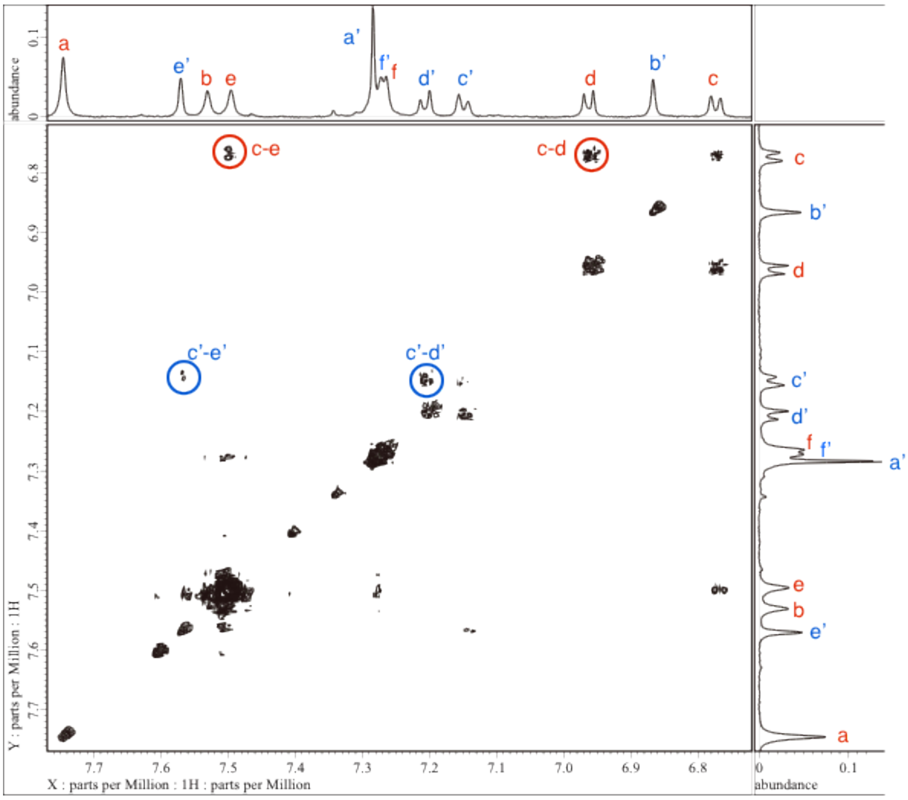

Figure S3. ^{1}H-^{1}H COSY spectrum of ($\mathbf{1}_{R,R}$-Ni)$_2$Pd (600 MHz,THF-d_8:CD$_3$CN = 5:1, TMS, 323 K)

It is inferred that the absence of cross peaks between the resonances a’ and e’ supports the *cis*-isomer of the Pd-β-diketonate moiety rather than the *trans* isomer, because the resonances of a’ and e’ in the *trans* isomer would be within the distance range to show a coupling (See Fig. S24).

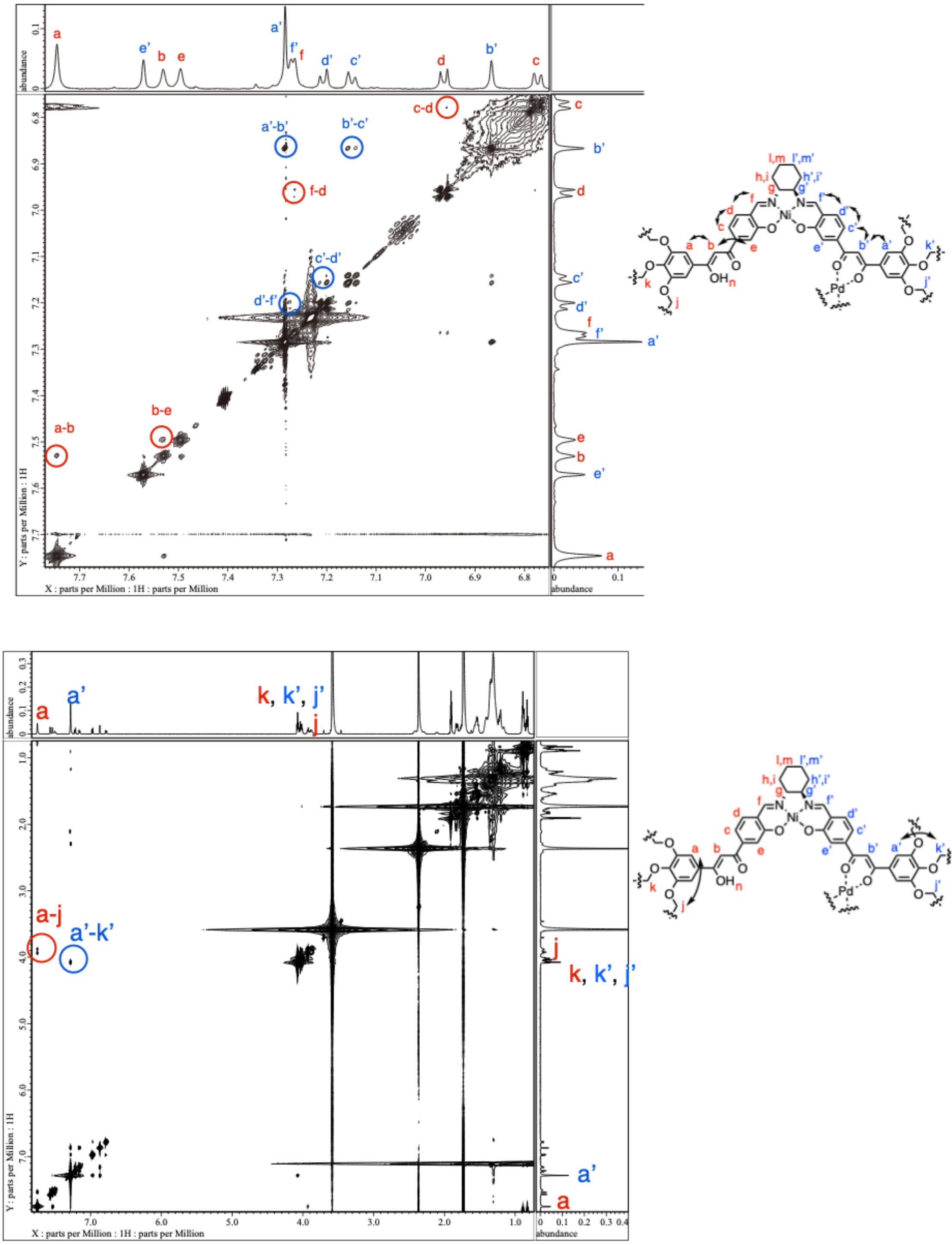

Figure S4. NOESY spectrum of ($\mathbf{1}_{R,R}$-Ni)$_2$Pd (600 MHz,THF-d_8:CD$_3$CN = 5:1, TMS, 323 K)

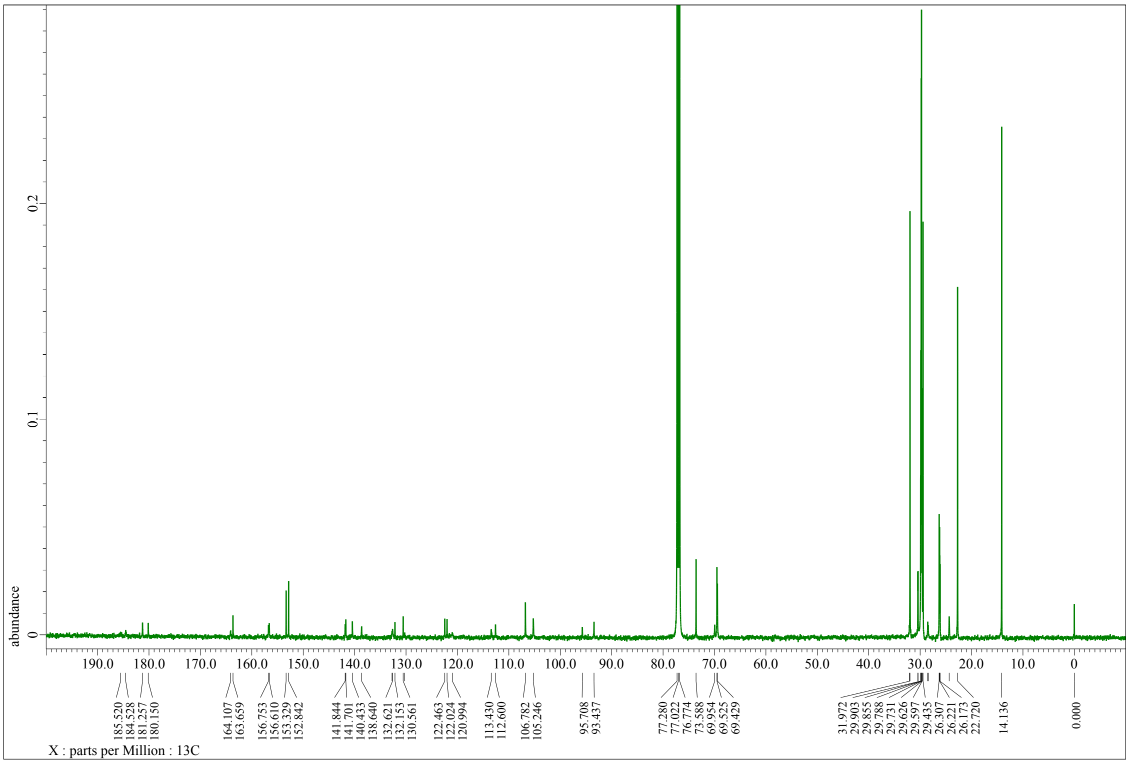

Figure S5. ^{13}C NMR spectrum of ($\mathbf{1}_{R,R}$-Ni)$_2$Pd (125 MHz, CDCl$_3$, TMS)

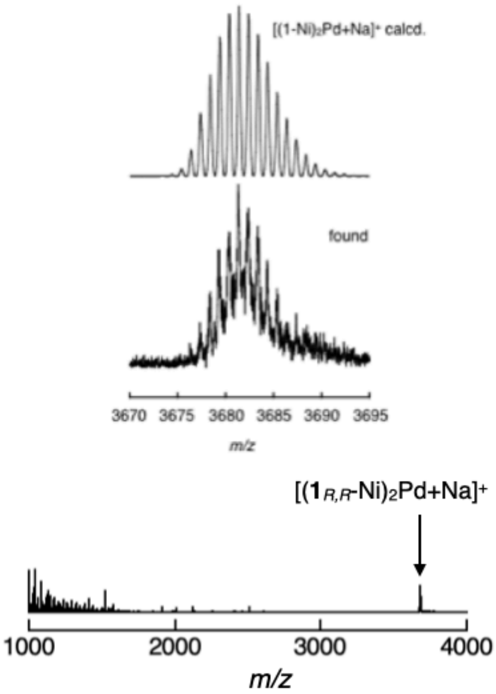

Figure S6. ESI-TOF MS spectrum of ($\mathbf{1}_{R,R}$-Ni)$_2$Pd

3. Thermogravimetric analysis (TGA)

TGA of **1**$_{R,R}$-Ni, **1**$_{S,S}$-Ni, and **1**$_{R,R}$-Pd were carried out by TA instruments TGAQ50 under nitrogen atmosphere. The sample was placed on the platinum sample holder. The temperature was increased at a rate of 10 °C/min unitl 600 °C. The TGA results indicated that the **1**$_{R,R}$-Ni, **1**$_{S,S}$-Ni, and **1**$_{R,R}$-Pd were stable up to 333 °C, 320 °C, and 280 °C, respectively.

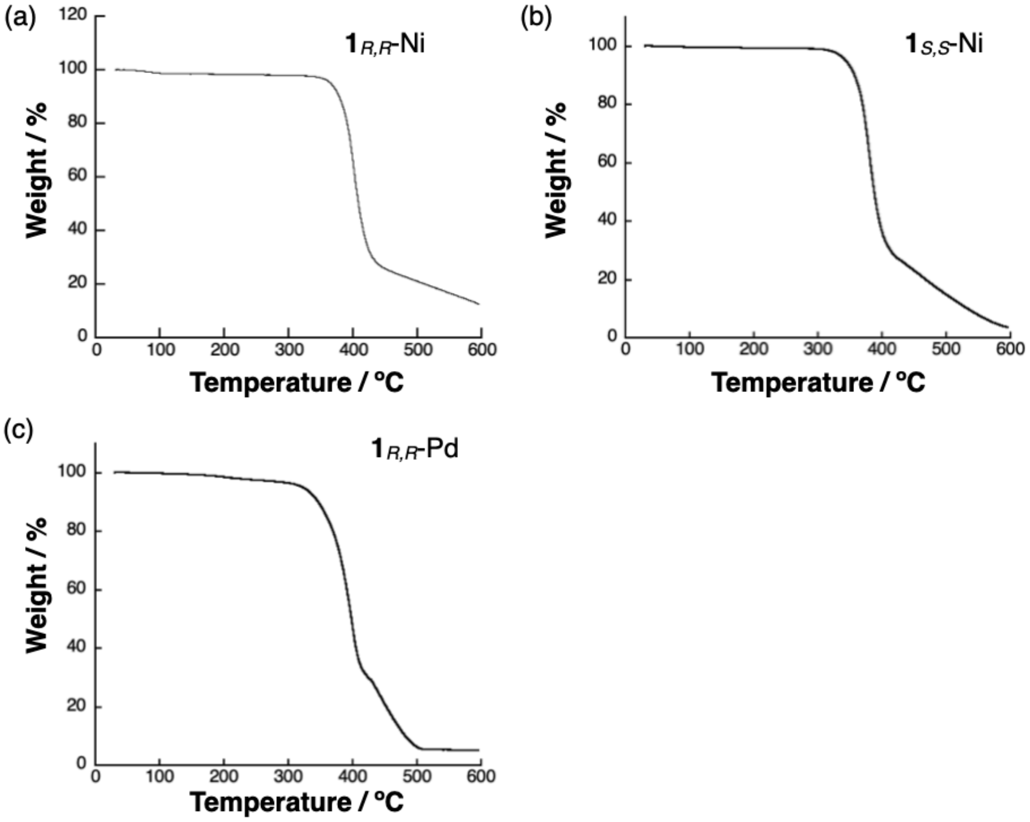

Figure S7. TGA of (a) **1**$_{R,R}$-Ni, (b) **1**$_{S,S}$-Ni, and (c) **1**$_{R,R}$-Pd

4. Differential scanning calorimetry (DSC)

DSC measurements were carried out under N_2 atmosphere with TA Instruments Q2000 DSC equipped with a RCS 90 cooling accessory and the transition temperatures were determined from the second heating run at a rate of 10 °C/min using Universal Analysis 2000 software.

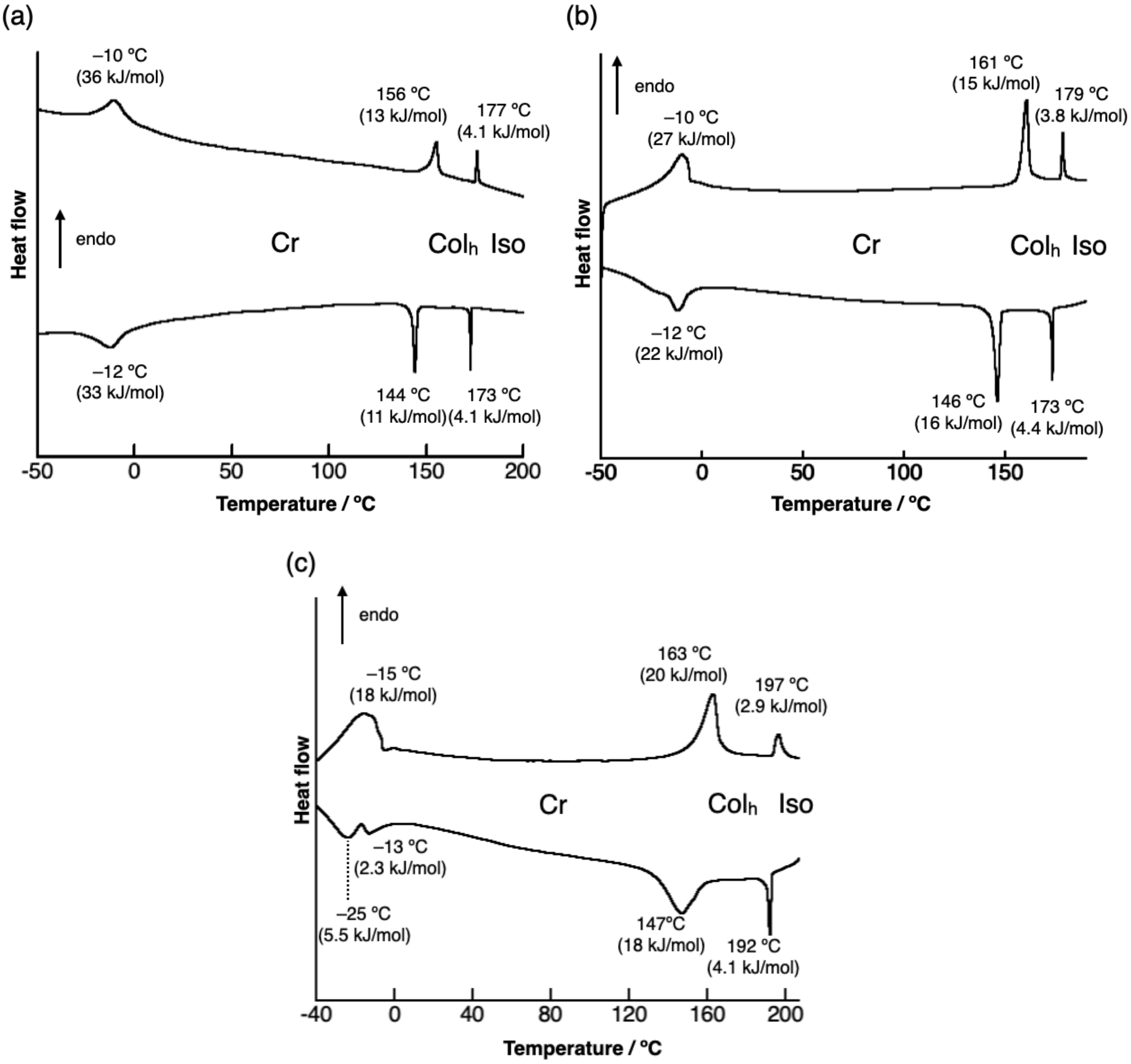

Figure S8. DSC profiles of of **1**$_{R,R}$-Ni, (b) **1**$_{S,S}$-Ni, and (c) **1**$_{R,R}$-Pd

5. Polarized optical microscopy

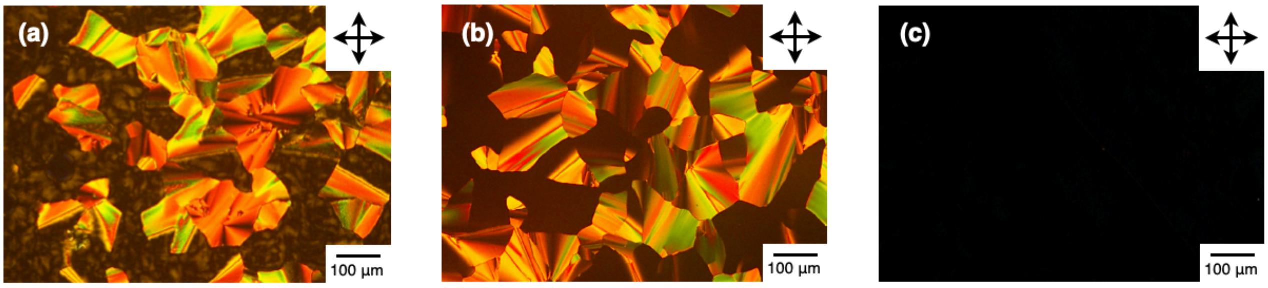

Figure S9. POM images of **1**$_{R,R}$-Ni at (a) 22 °C, (b) 171 °C, and (c) 182 °C.

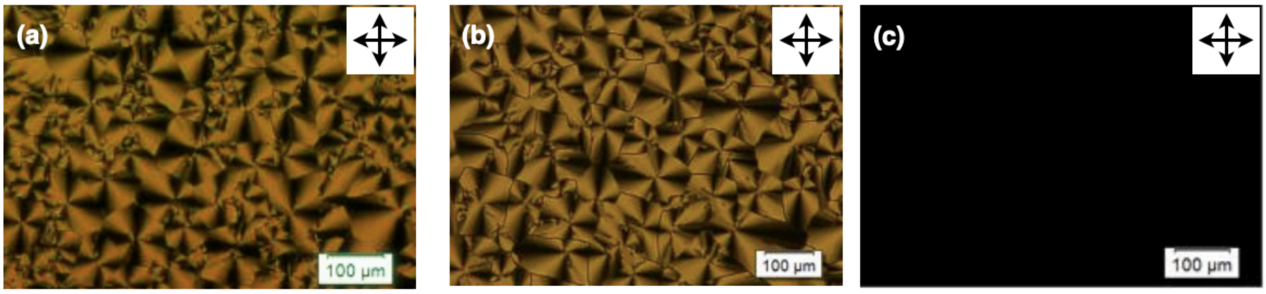

Figure S10. POM images of **1**$_{S,S}$-Ni at (a) 20 °C, (b) 170 °C, and (c) 180 °C.

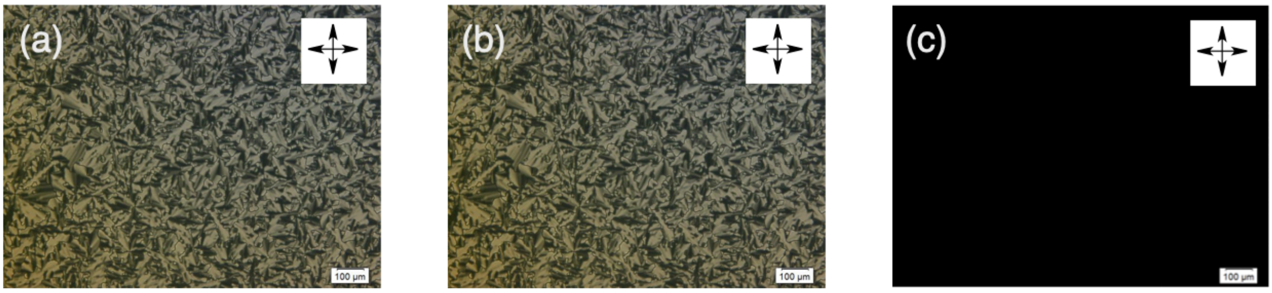

Figure S11. POM images of **1**$_{R,R}$-Pd at (a) 22 °C, (b) 170 °C, and (c) 215 °C.

6. Structural analysis using XRD

6-1. GIXRD patterns of the $\mathbf{1}_{R,R}$-Ni at different temperatures

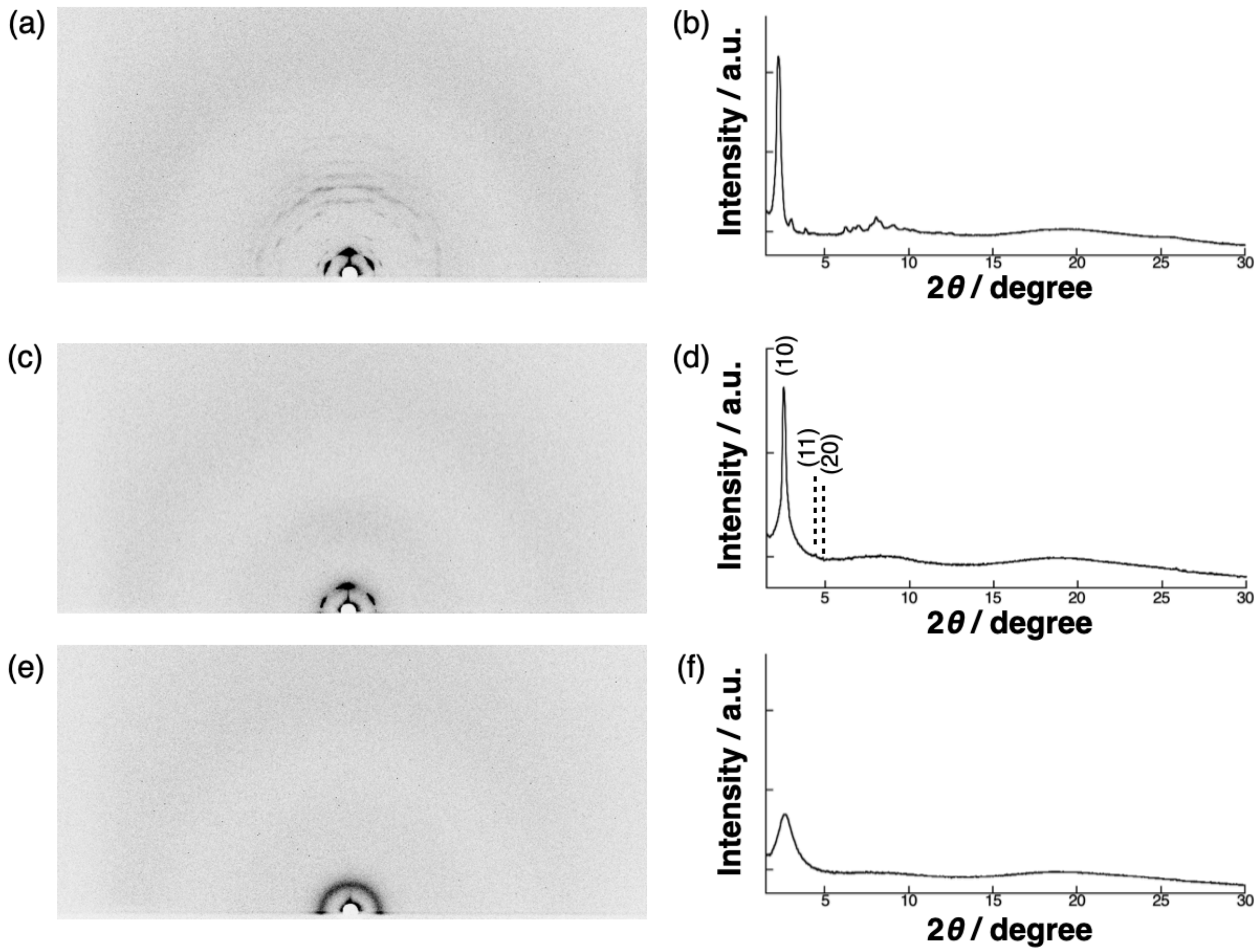

Figure S12. X-ray diffraction patterns in GIXRD for $\mathbf{1}_{R,R}$-Ni at (a), (b) 96 ºC; (c), (d) 163 °C; and (e), (f) 186 °C.

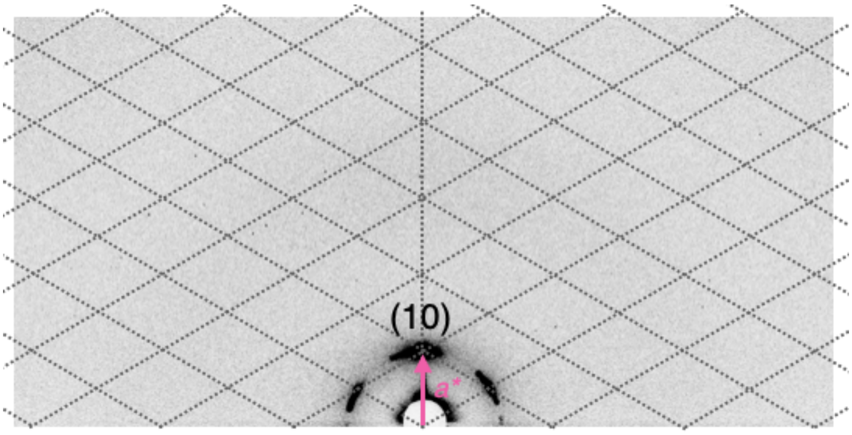

Figure S13. X-ray diffraction patterns in GIXRD for $\mathbf{1}_{R,R}$-Ni at 163 °C.

Table S1. Observed GIXRD data of the liquid crystalline phases of $\mathbf{1}_{R,R}$-Ni, diffraction angles $2\theta_{\mathrm{obs}}$ (º), Miller indices *h,k,l, d* value d_{obs} (Å), d_{calc} (Å) are *d* values calculated from the lattice parameters of $\mathbf{1}_{R,R}$-Ni at 96 °C and 163 °C.

Temperature (ºC)	$2\theta_{\mathrm{obs}}$ (º)	*hk*	d_{obs} (Å)	d_{calc} (Å)	$d_{\mathrm{obs}} - d_{\mathrm{calc}}$ (Å)	2D cell parameter
96	2.24	(10)	39.4	–	–	Cr *a* = 45.6 Å
	3.01		29.3			
	3.88	(11)	22.8	22.7	0.1	
	4.41	(20)	20.0	19.7	0.3	
	6.26	(21)	14.1	14.9	–0.8	
	6.74	(30)	13.1	13.1	0.0	
	7.00		12.6			
	8.05	(22)	11.0	11.4	−0.4	
	8.28	(31)	10.7	10.9	−0.2	
	9.07	(40)	9.7	9.9	−0.11	
	9.74	(32)	9.1	9.0	0.1	
	10.2	(41)	8.6	8.6	0.03	
	11.8	(50)	7.5	7.88	−0.38	
	12.5	(42)	7.1	7.4	−0.4	
163	2.53	(10)	34.9	–	–	Col$_{\mathrm{h}}$ *a* = 39.8 Å
	4.43	(11)	19.9	20.1	–0.21	
	4.87	(20)	18.1	17.4	–0.68	

6-2. GIXRD patterns of the **1**$_{S,S}$-Ni at different temperatures

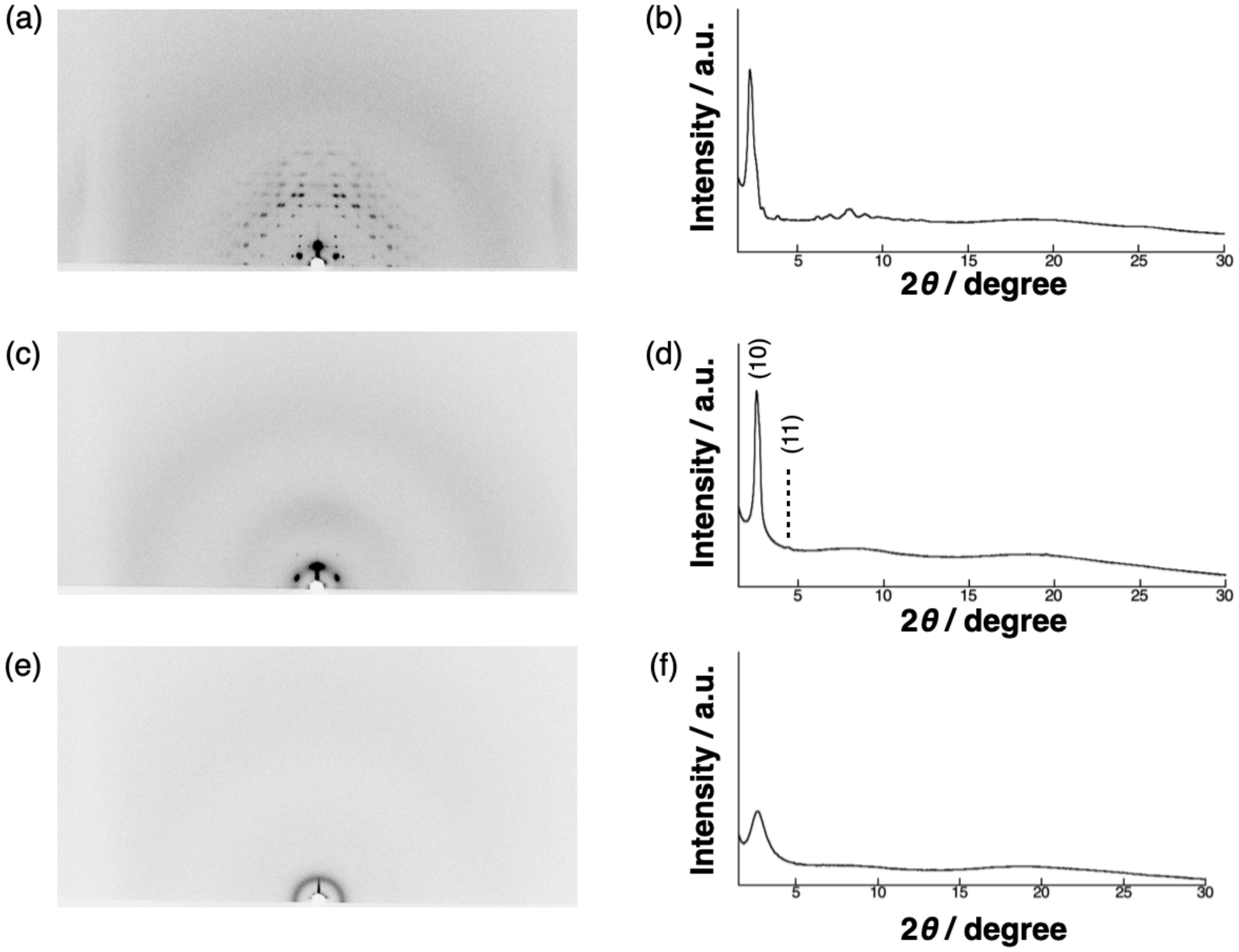

Figure S14. X-ray diffraction patterns in GIXRD for **1**$_{S,S}$-Ni at (a), (b) 100 ºC; (c), (d) 164 °C; and (e), (f) 188 °C.

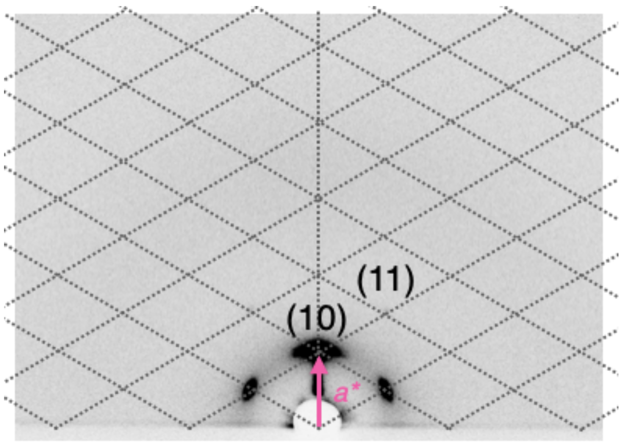

Figure S15. X-ray diffraction patterns in GIXRD for **1**$_{S,S}$-Ni at 164 °C.

Table S2. Observed GIXRD data of the liquid crystalline phases of $\mathbf{1}_{S,S}$-Ni, diffraction angles $2\theta_{\mathrm{obs}}$ (º), Miller indices *h,k,l, d* value d_{obs} (Å), d_{calc} (Å) are *d* values calculated from the lattice parameters of $\mathbf{1}_{S,S}$-Ni at 100 °C and 164 °C.

Temperature (ºC)	$2\theta_{\mathrm{obs}}$ (º)	*hk*	d_{obs} (Å)	d_{calc} (Å)	$d_{\mathrm{obs}} - d_{\mathrm{calc}}$ (Å)	2D cell parameter
100	2.22	(10)	39.8	–	–	Cr
	2.97		29.7			*a* = 46.0 Å
	3.84	(11)	23.0	23.0	0	
	6.18	(21)	14.3	15.0	–0.7	
	6.67	(30)	13.2	13.3	-0.1	
	6.92		12.8			
	7.96	(22)	11.1	11.5	−0.4	
	8.08	(31)	10.9	11.0	−0.1	
	8.97	(40)	9.8	9.9	−0.1	
	9.71	(32)	9.1	9.1	0	
	10.3	(41)	8.6	8.7	−0.1	
	10.9	(50)	8.1	8.0	0.1	
	11.7	(33)	7.6	7.7	−0.1	
	12.3	(42)	7.1	7.5	−0.4	
164	2.56	(10)	34.5	–	–	$\mathrm{Col_h}$
	4.35	(11)	20.3	19.9	0.40	*a* = 40.6 Å

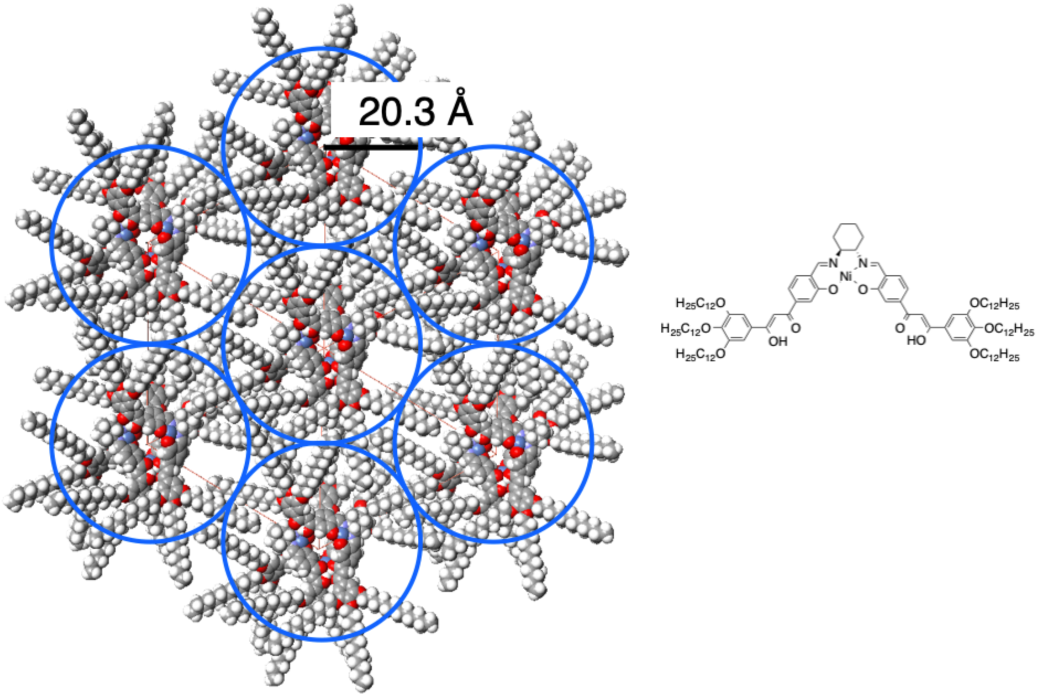

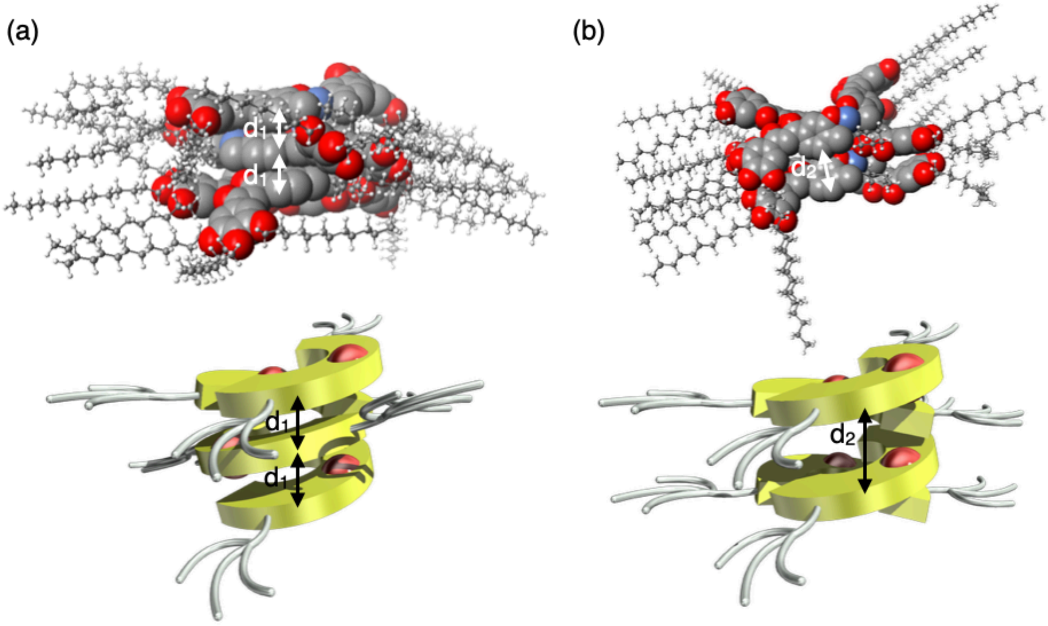

Figure S16. Tentative model of the packing structure of $\mathbf{1}_{S,S}$-Ni in the liquid-crystalline phase. (a) A side view of the helical columnar structure of $\mathbf{1}_{S,S}$-Ni. (b) The another stacking structure with a periodicity of folded dimer. The aromatic carbons, Ni ion, and oxygens are presented as the van der Waals model.

Given that the postulated density, ρ of the molecule is approximately 1 g/cm^3, the cell parameter of 2.0 nm suggested by GIXRD results indicates the molecular number Z is estimated to be 1.7, where $Z = \rho VN/\mathrm{M_w}$ (V = volume, $N_{\mathrm{Avogadro\ number}} = 6.02 \times 10^{23}$ mol^{-1}, M_w = molecular weight).[2] This result indicates that a dimer of the molecules stacks themselves in a helical fashion to form the hexagonal packing as shown in Figure S16. In the postulated structure, the right-handed helical structure has stacking distances, d_1 between the Ni-salen moieties or between Ni-salen-β-diketone moieties of 0.32–0.34 nm and 0.33–0.35 nm, respecticely (Figure S16a). On the other hand, the another possible stacking structure with a periodicity ascribed to the dimer of the $\mathbf{1}_{S,S}$-Ni has a periodic distance, $d_2 = 5.5$ nm (Figure S16b). The PXRD results (vide infra) support the former packing structure. In the helical stacking structgure, the intermolecular hydrogen bonding involving β-diketonate moiety might take place to form the helix as suggested in the other compounds possessing β-diketone moiety, albeit the contribution of the interaction seems to be small.[3,4]

6-3. PXRD patterns of the one-axiallly oriented sample of $\mathbf{1}_{S,S}$-Ni

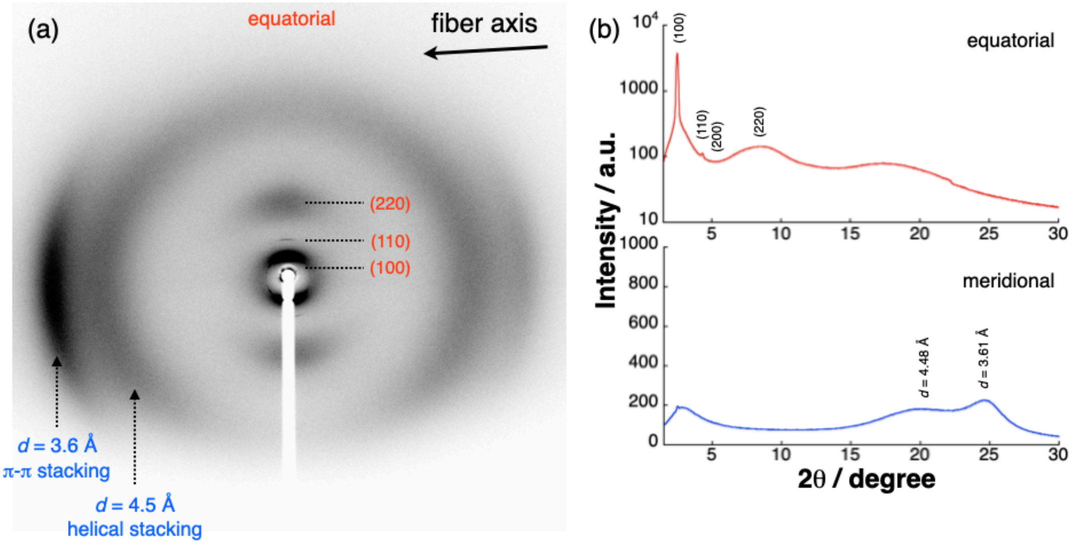

Figure S17. (a) 2D XRD pattern of the one-dimensionally aligned sample of $\mathbf{1}_{S,S}$-Ni at 164 °C. (b) 2theta–intensity profiles in the equatorial (top) and meridional (bottom) directions.

6-4. GIXRD patterns of the **1**$_{R,R}$-Pd at different temperatures

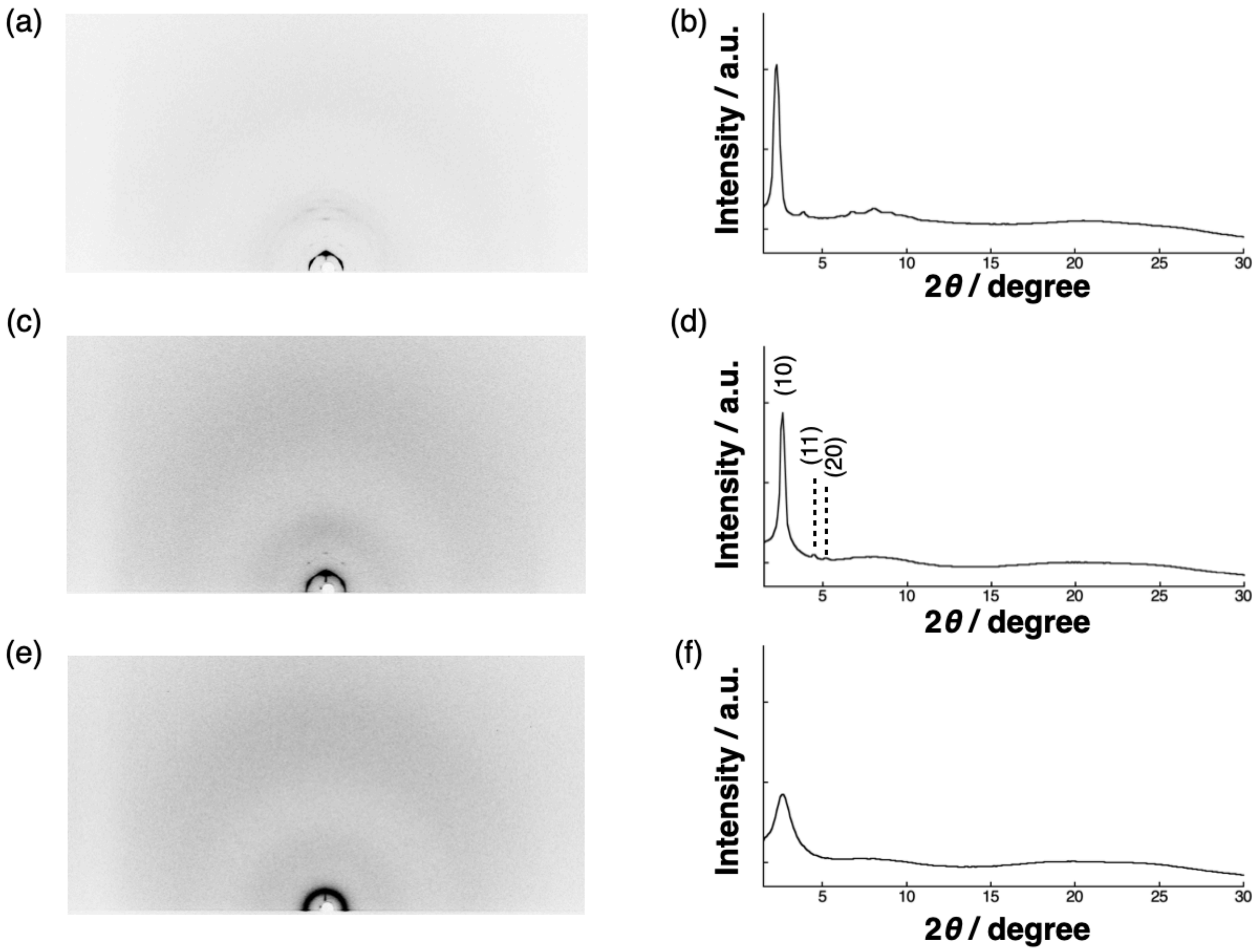

Figure S18. X-ray diffraction patterns in GIXRD for **1**$_{R,R}$-Pd at (a), (b) 28 ºC; (c), (d) 180 °C; and (e), (f) 200 °C.

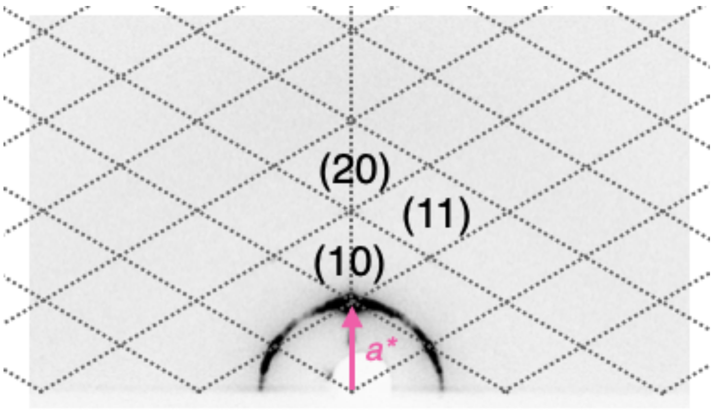

Figure S19. X-ray diffraction pattern in GIXRD for **1**$_{R,R}$-Pd at 180 °C.

Table S3. Observed GIXRD data of the liquid crystalline phases of **1**$_{R,R}$-Pd, diffraction angles $2\theta_{obs}$ (º), Miller indices *h,k,l, d* value d_{obs} (Å), d_{calc} (Å) are *d* values calculated from the lattice parameters of **1**$_{R,R}$-Pd at 28 °C and 180 °C.

Temperature (ºC)	$2\theta_{obs}$ (º)	*hk*	d_{obs} (Å)	d_{calc} (Å)	$d_{obs} - d_{calc}$ (Å)	2D cell parameter
28	2.27	(10)	38.9	–	–	Cr *a* = 45.4 Å
	3.89	(11)	22.7	22.5	0.24	
	4.50	(20)	19.6	19.4	0.30	
	6.11	(21)	14.5	14.7	–0.2	
	6.78	(30)	13.0	13.0	0.06	
	8.08	(22)	10.9	11.2	0.3	
	8.97	(40)	9.85	9.72	0.13	
	9.88	(32)	8.94	8.92	0.02	
	10.2	(41)	8.66	8.49	0.17	
	11.2	(33)	7.89	7.49	0.40	
180	2.60	(10)	34.0	–	–	Col_h *a* = 39.6 Å
	4.45	(11)	19.8	19.6	0.20	
	5.15	(20)	17.1	17.0	0.1	

7. Infrared (IR) spectroscopy

7-1. IR spectrum of $\mathbf{1}_{S,S}$-Ni

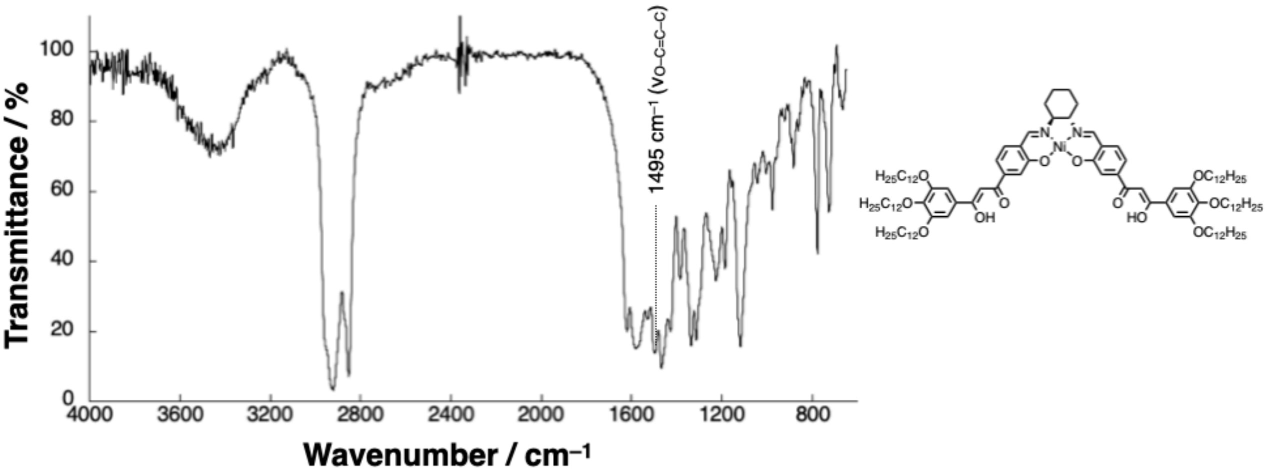

Figure S20. IR spectrum of $\mathbf{1}_{S,S}$-Ni at 22 °C (KBr method).

7-2. Microscopic polarized IR measurement of **1**$_{R,R}$-Ni

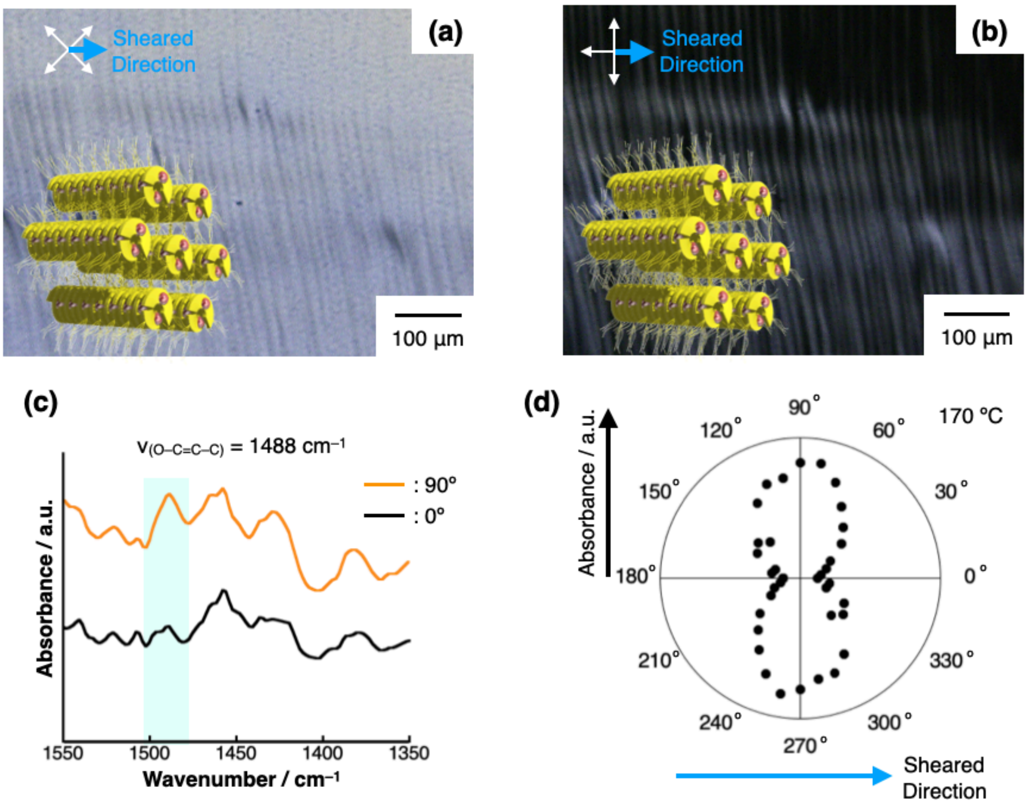

Figure S21. POM images of the sheared sample of **1**$_{R,R}$-Ni at 22 °C with the polarizer set to (a) 45° and (b) 0° to the sheared direction. (c) Microscopic IR spectra recorded at 170 °C. The polarized light is set to 90° (orange line) and 0° (black line) to the shearing direction (d) Polar plot of the β-diketonate O–C=C–C stretching band of **1**$_{R,R}$-Ni.

As shown in Figure S21, POM image of the sheared sample showed a homogeneous bright birefringence with the sheared direction oriented by 45° to the polarizers. In contrast, when the sheared direction was set parallel to the one of the polarizers, the dark image was observed. These results indicate the columnar assembly of **1**$_{R,R}$-Ni could be readily aligned to the sheared direction. In microscopic IR spectra of **1**$_{R,R}$-Ni at the LC state, a peak corresponding to the O–C=C–C stretching of acetylacetonate moiety coupled with in-plane bending OH band appear around at 1488 cm^{-1}. The O–C=C–C stretching bond have a maximum when the polarizer is set to 90° with respect to the sheared direction. Relatively large dichroic ratio ($A_{\parallel}/A_{\perp}$) of 2.4 in the absorbance regarding the O–C=C–C stretching band was observed. The results clearly illustrate that the planar mesogen of Ni-salen moiety orients perpendicular to the long axis of the columnar assembly.

8. Structural analysis of (**1**$_{R,R}$-Ni)$_2$Pd

8-1. Comparison of ^{1}H NMR spectra of **1**$_{R,R}$-Ni and (**1**$_{R,R}$-Ni)$_2$Pd

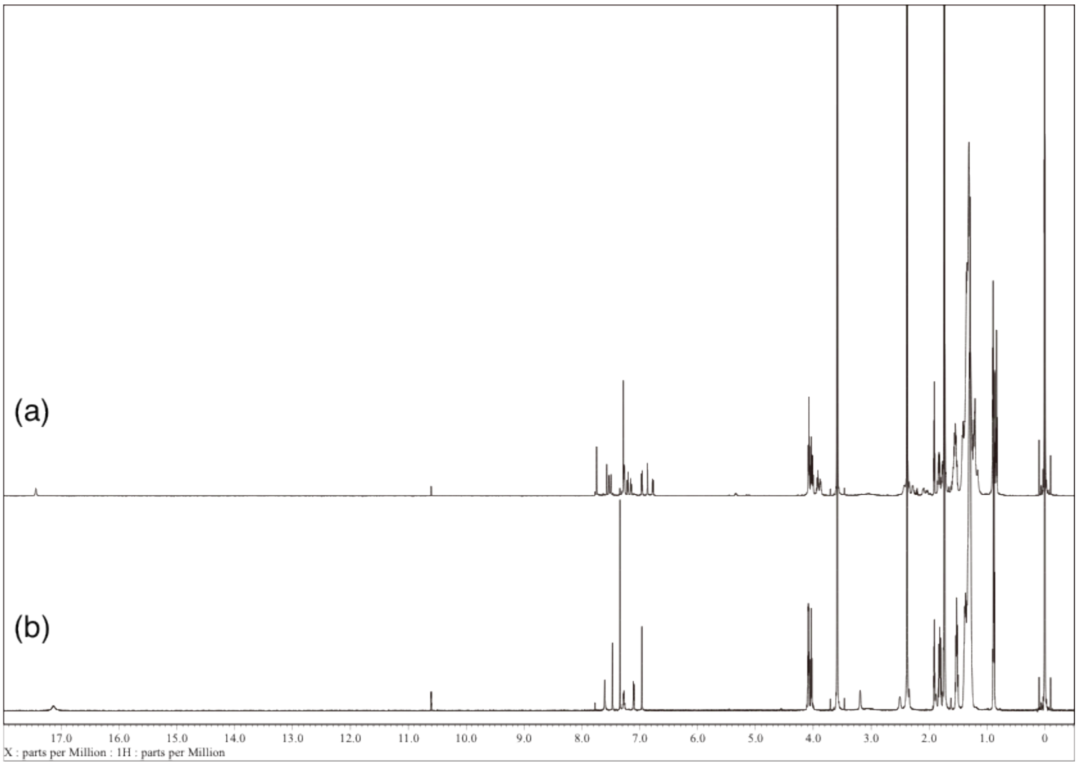

Figure S22. ^{1}H NMR spectra of (a)(**1**$_{R,R}$-Ni)$_2$Pd and (b) **1**$_{R,R}$-Ni (600 MHz,THF-d_8:CD$_3$CN = 5:1, TMS, 323 K)

8-2. Concentration dependece of ^{1}H NMR spectra of $(\mathbf{1}_{R,R}\text{-Ni})_2$Pd

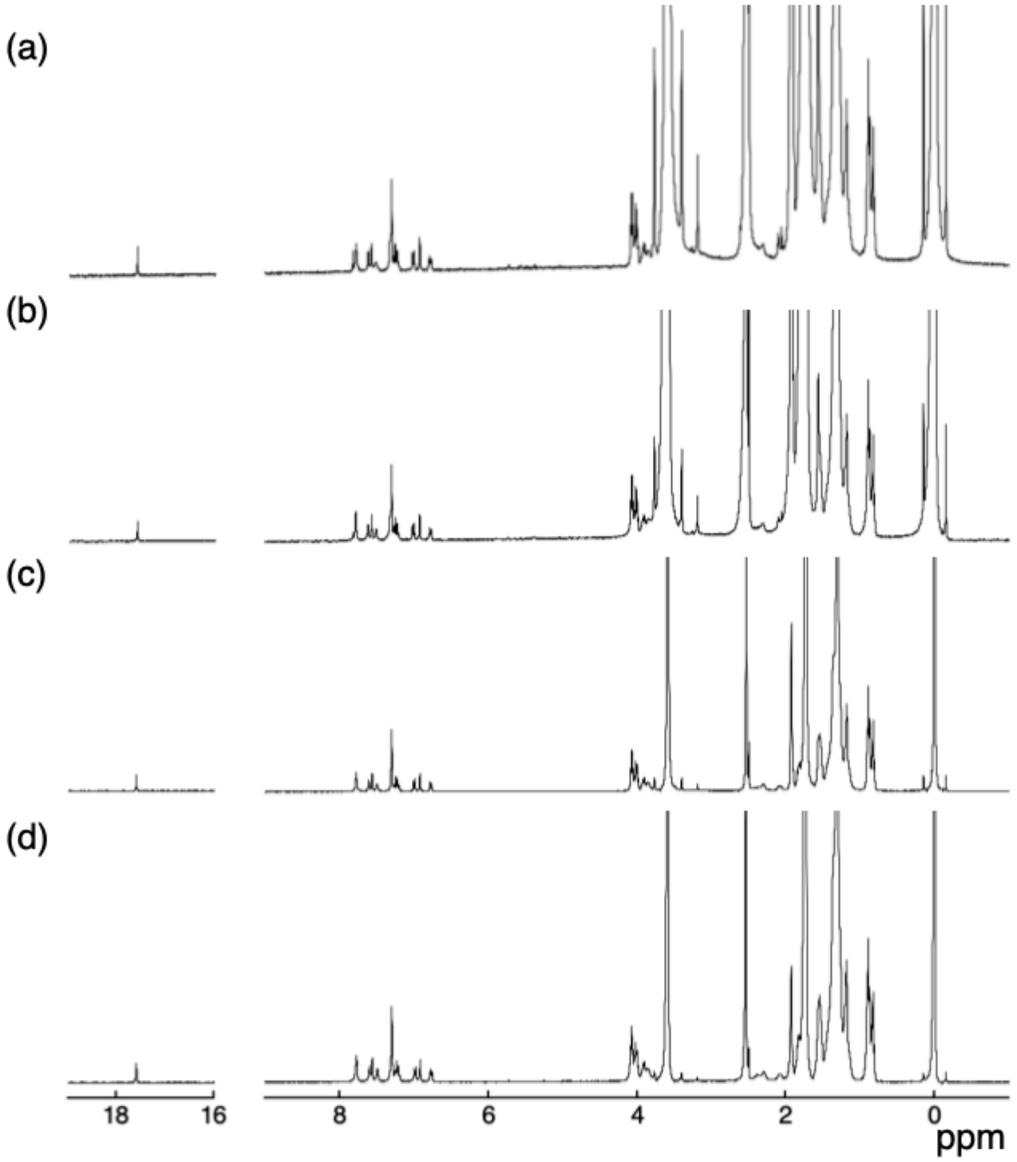

Figure S23. Concentration dependence of ^{1}H NMR spectra of $(\mathbf{1}_{R,R}\text{-Ni})_2$Pd (400 MHz,THF-$d_8$:$CD_3CN$ = 5:1, TMS, 293 K) (a) 0.05 mM, (b) 0.1 mM, (c) 0.5 mM, and (d) 1.0 mM.

8-3. Modelling of ($\mathbf{1}_{R,R}$-Ni)$_2$Pd

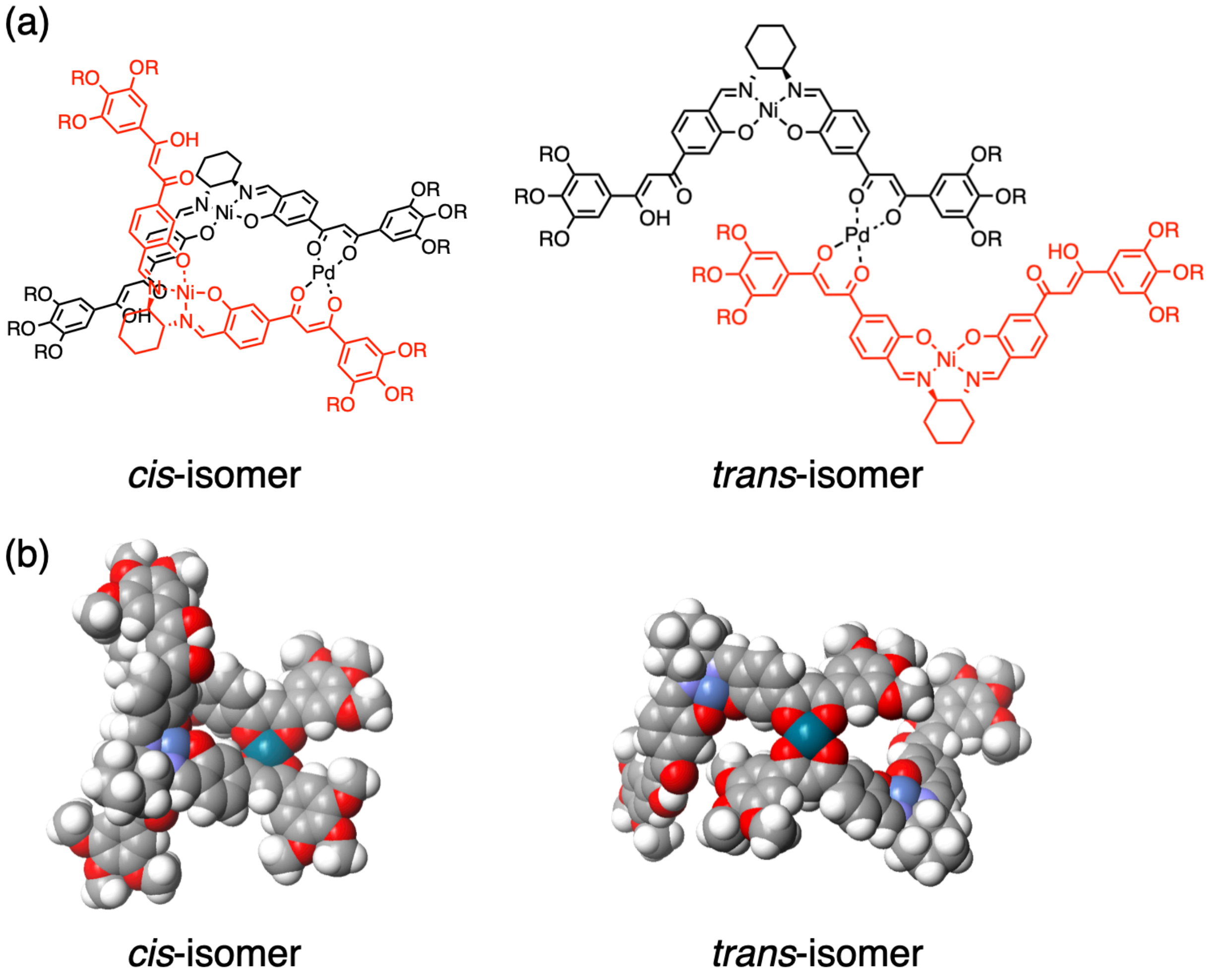

Figure S24. (a) Chemical structures of *cis* and *trans* isomers of ($\mathbf{1}_{R,R}$-Ni)$_2$Pd. (b) Model structrues calculated by molecular mechanics (MM2) of *cis* and *trans* isomers of ($\mathbf{1}_{R,R}$-Ni)$_2$Pd. For simplification of the calculation, the dodecyl chains were substituted with methyl groups.

8-4. DFT calculation of $(\mathbf{1}_{R,R}\text{-Ni})_2\text{Pd}$

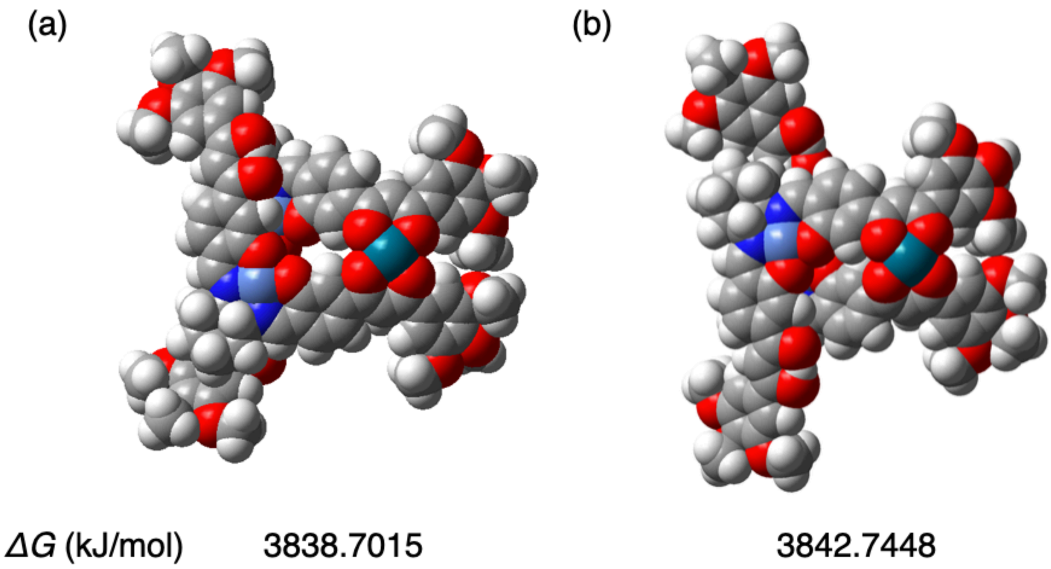

Figure S25. Optimized structures of (a) *M*- and (b) *P*-helix of the $(\mathbf{1}_{R,R}\text{-Ni})_2\text{Pd}$ calculated by the density functional theory (DFT) method at the B3LYP/6-31G (d) level of theoly.

The molecular structures of *M*- and *P*-helix isomers of the $(\mathbf{1}_{R,R}\text{-Ni})_2\text{Pd}$ were optimized by the density functional theory (DFT) method at the B3LYP/6-31G (d) level of theory, employing the basis sets of 6-31G(d) for C, H, N, O, SDD for Ni, and Pd, respectively. The basis function was combined with the dispersion correction (D3BJ).[5] The dodecyl chains were substituted with methyl groups for simplification. The optimized structures were confirmed that they do not have imaginary frequencies by normal mode analyses. The DFT calculation suggested that the *M*-isomer is preferable than that of the *P*-isomer (ΔE = –4.0 kJ/mol).

8-5. VT NMR of $(\mathbf{1}_{R,R}\text{-Ni})_2\text{Pd}$

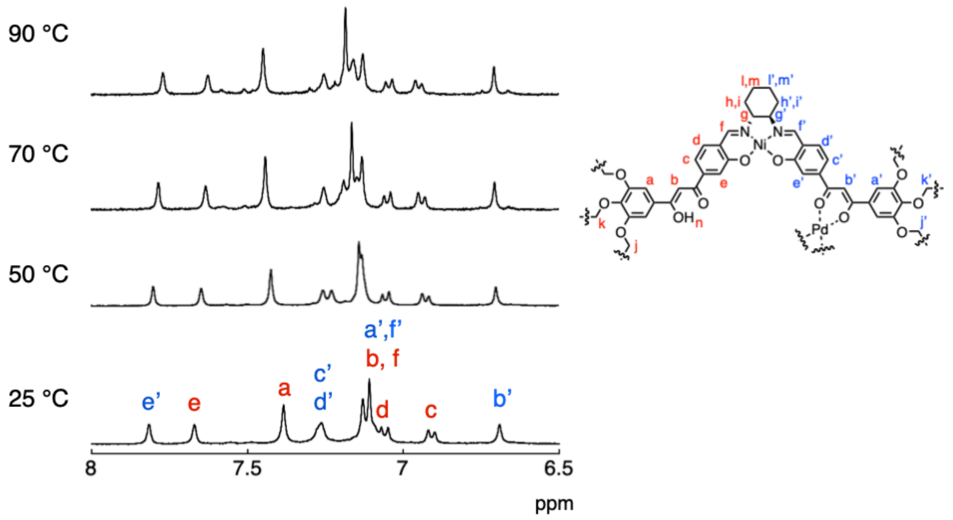

Figure S26. VT NMR spectra of $(\mathbf{1}_{R,R}\text{-Ni})_2\text{Pd}$ at temperatures of 25 to 120 °C in tetrachloroethane-d_2.

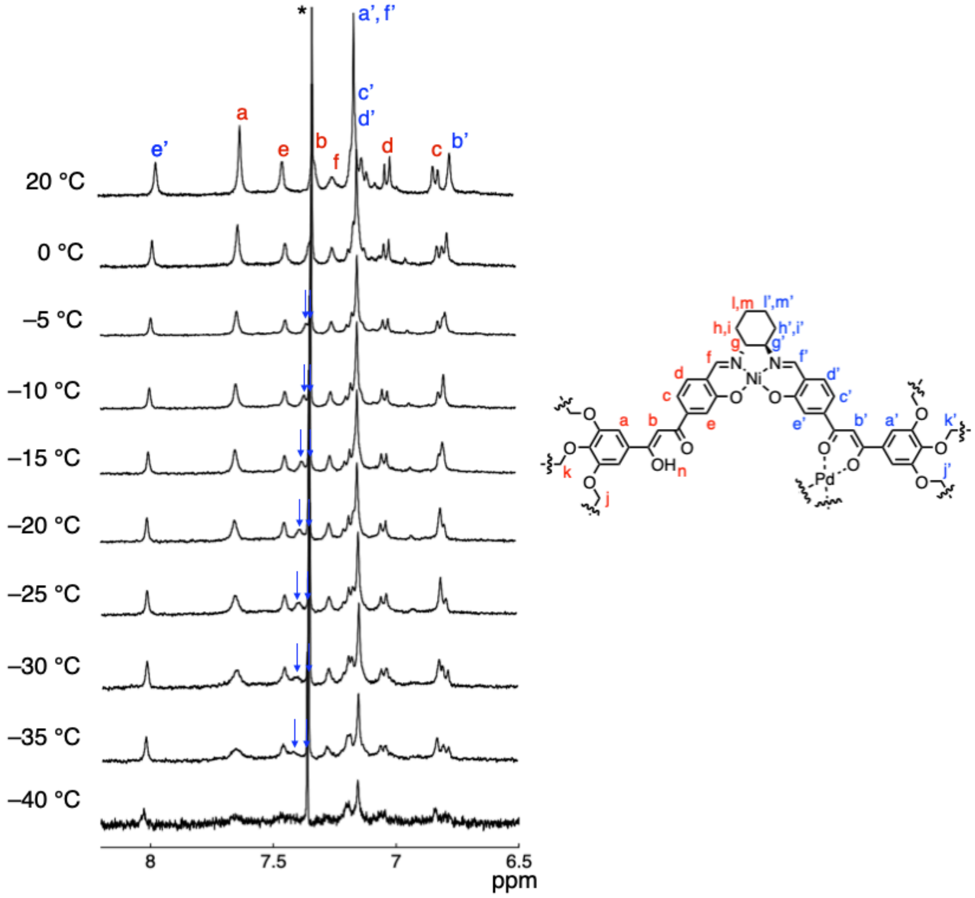

Figure S27. VT NMR spectra of $(\mathbf{1}_{R,R}\text{-Ni})_2\text{Pd}$ at temperatures of 20 to –40 °C in CD_2Cl_2.

Upon cooling to –40 °C, the ^{1}H NMR signals of ($\mathbf{1}_{R,R}$-Ni)$_2$Pd did not split except the proton b that is ascribled to methine moieties in the non-chelating β-diketone. The other signals became broad below –40 ºC. The splitting of the b proton might be attributed to the difference on orientation of the side chains due to the rotation of the C-C bond between the β-diketonate and the benzene in the Ni-salen moiety.

8-6. CD and UV-vis spectra

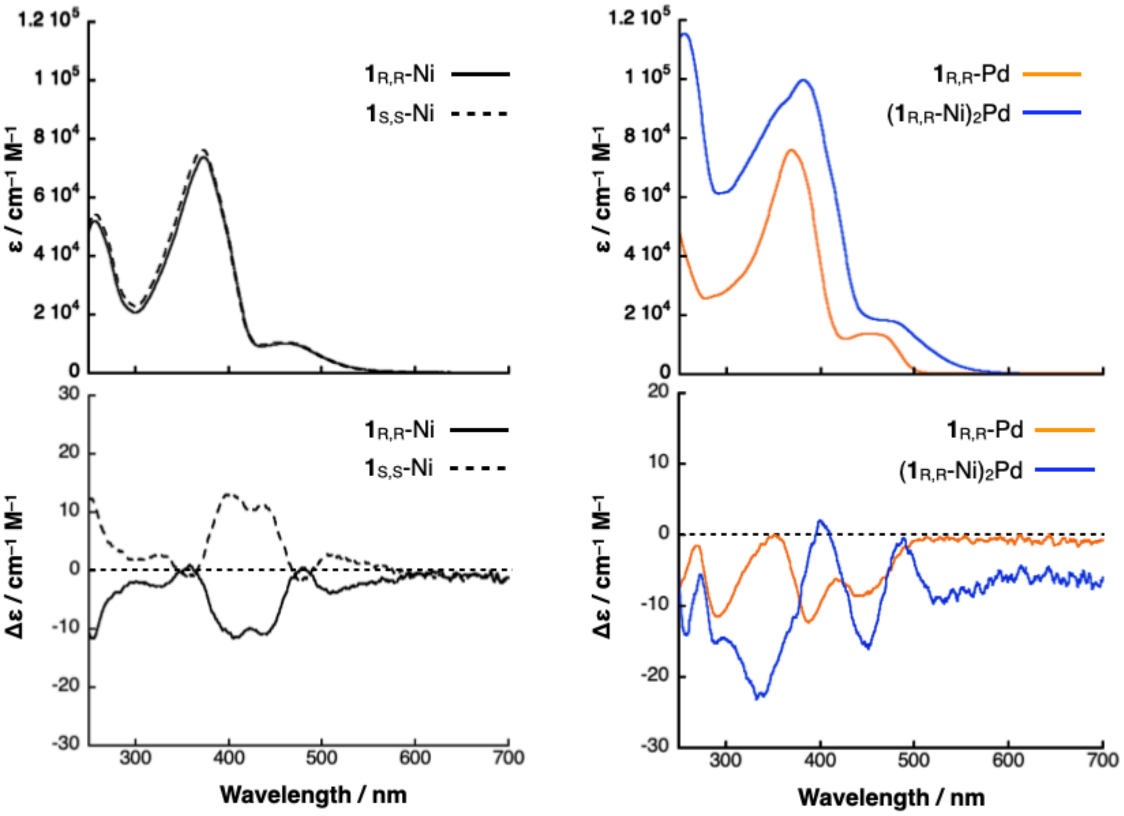

Figure S28. CD and UV-vis spectra $\mathbf{1}_{R,R}$-Ni (black solid), $\mathbf{1}_{S,S}$-Ni (black dashed line), $\mathbf{1}_{R,R}$-Pd (orange solid), and ($\mathbf{1}_{R,R}$-Ni)$_2$Pd (blue solid) at 50 °C in THF:CD$_3$CN = 5:1. [**1**-Ni or **1**-Pd] and [($\mathbf{1}_{R,R}$-Ni)$_2$Pd] are 12×10^{-6} M and 6×10^{-6} M, respectively.

As shown in Fgiure S28, $\mathbf{1}_{R,R}$-Ni and $\mathbf{1}_{S,S}$-Ni exhibit the opposite CD pattern related to the MLCT bands at 405-438 nm, whereas ($\mathbf{1}_{R,R}$-Ni)$_2$Pd exhibits the negative CD bands at 336 and 450 nm followed by a broad negative band at 530 nm.

8-7. DFT calculation of ECD spectra

The molecular structures of *M*-helix and *P*-helix of ($\mathbf{1}_{R,R}$-Ni)$_2$Pd were optimized by the density functional theory (DFT) method at the B3LYP/6-31G (d) level of theory, employing the basis sets of 6-31G(d) for C, H, N, O, and SDD for Ni and Pd, respectively. The dodecyl chains of ($\mathbf{1}_{R,R}$-Ni)$_2$Pd were substituted with methyl group for simplicity. The optimized structures were confirmed that they do not have imaginary frequencies by normal mode analyses. Excited states (S1 – S100) of those molecules were examined at the optimized geometry by the time-dependent DFT (TD-DFT) calculations using B3LYP/6-311G (d,p) employing a basis sets 6-311G (d,p) for C, H, N, O, and SDD for Ni, and Pd. TD-DFT calculation under a solvent (THF) condition with a polarizable continuum model (PCM) using the integral equation formalism variant (IEFPCM). All calculations were performed by Gaussian 16 program package.[6]

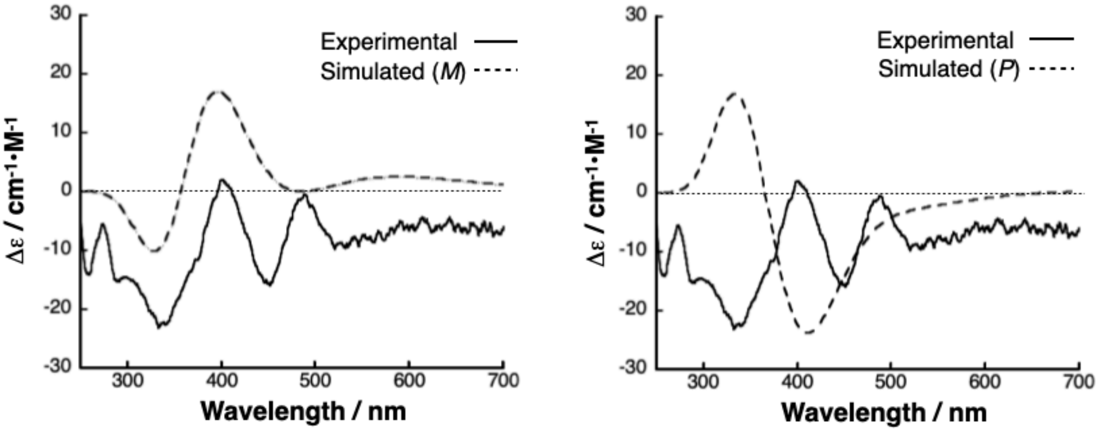

Figure S29. Experimental (solid) and simulated (dashed) CD spectra of ($\mathbf{1}_{R,R}$-Ni)$_2$Pd. Simulated (M) and Simulated (P) correspond to the (*M*)-helix and (*P*)-helix of ($\mathbf{1}_{R,R}$-Ni)$_2$Pd, respectively. Experimental spectra were obtained as shown in Figure S28.

8-8. Thermal property of $(\mathbf{1}_{R,R}\text{-Ni})_2\text{Pd}$

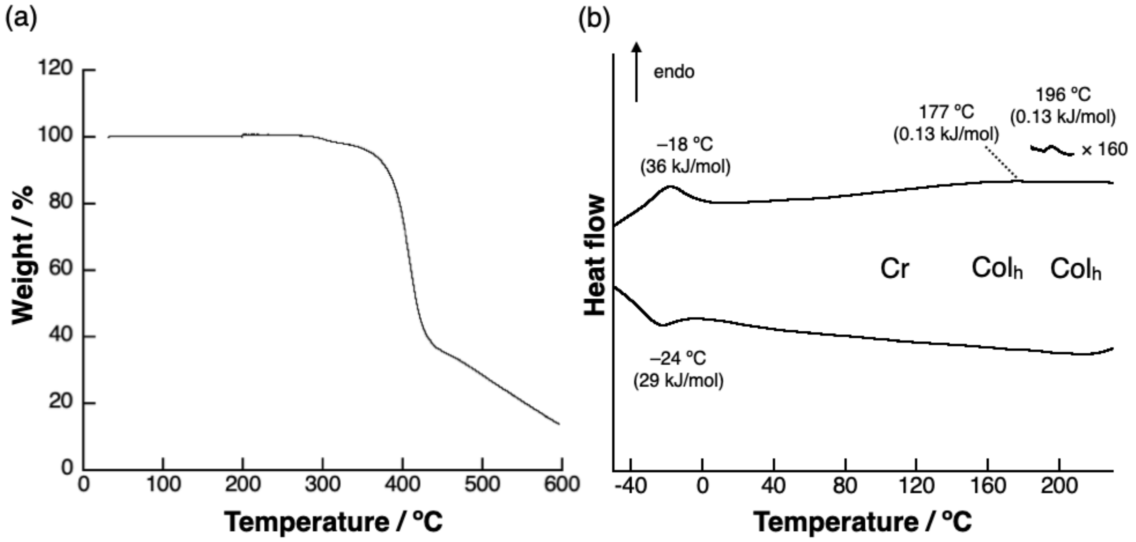

Figure S30. (a) TGA and (b) DSC profiles of $(\mathbf{1}_{R,R}\text{-Ni})_2\text{Pd}$. TGA profile indicates that $(\mathbf{1}_{R,R}\text{-Ni})_2\text{Pd}$ is stable up to 295 °C

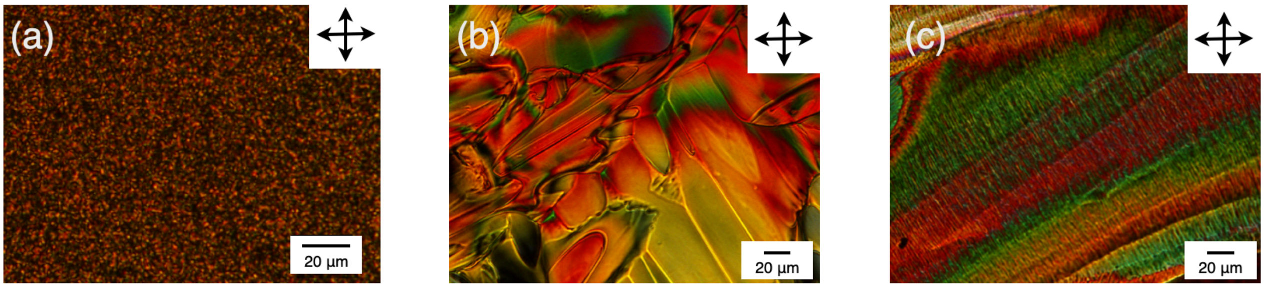

Figure S31. POM images of $(\mathbf{1}_{R,R}\text{-Ni})_2\text{Pd}$ at (a) 50 °C, and (b) 185 °C.and (c) 204 °C.

8-9. GIXRD patterns of $(\mathbf{1}_{R,R}\text{-Ni})_2\text{Pd}$ at different temperatures

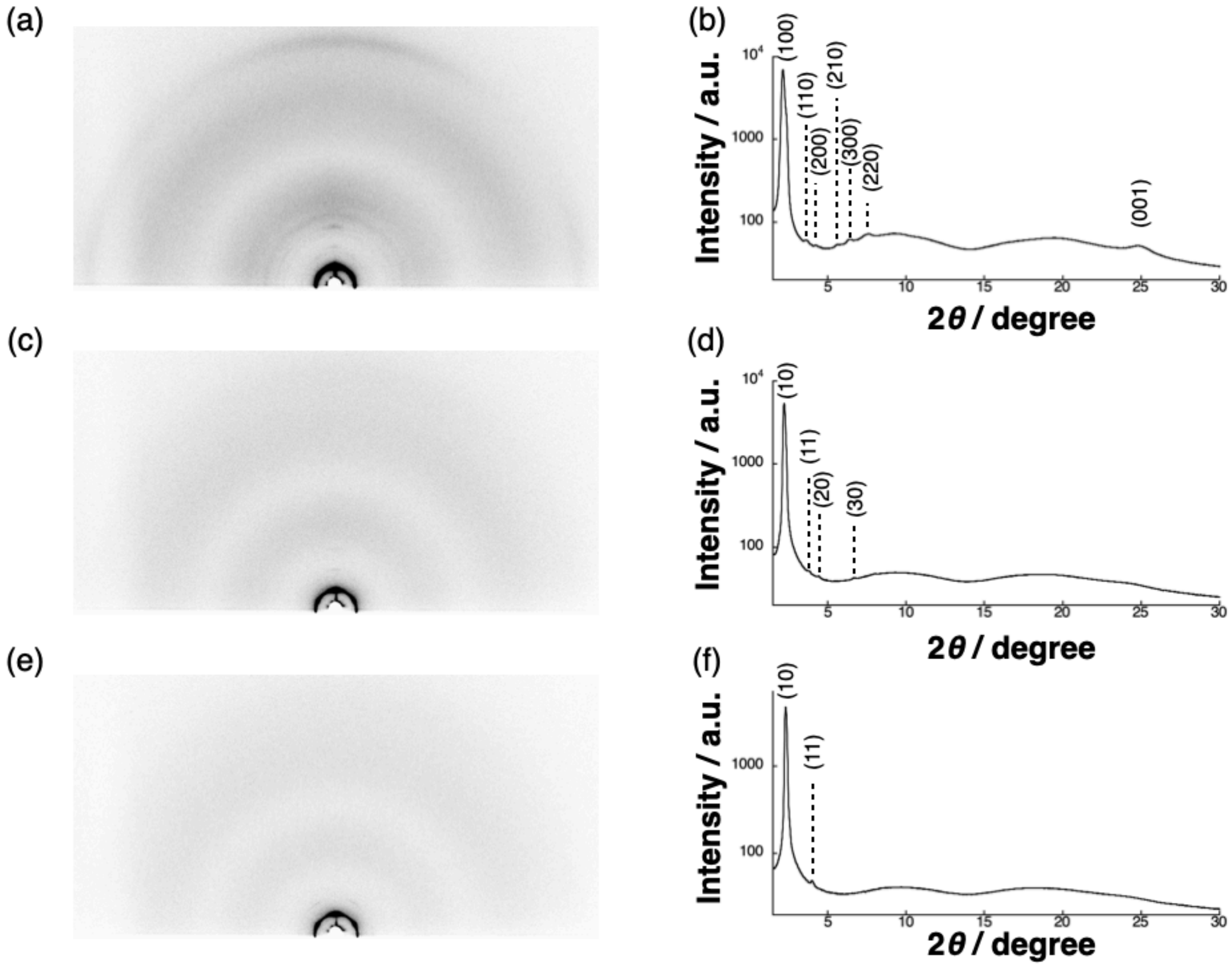

Figure S32. X-ray diffraction patterns in GIXRD for $(\mathbf{1}_{R,R}\text{-Ni})_2\text{Pd}$ at (a), (b) 100 ºC; and (c), (d) 185 °C, and (e), (f) 204 °C,

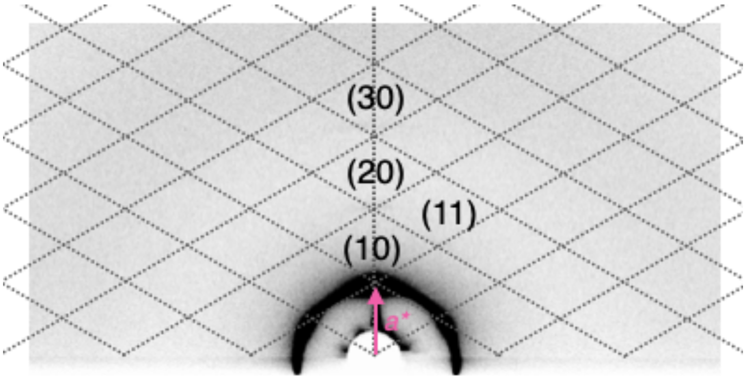

Figure S33. X-ray diffraction pattern in GIXRD for $(\mathbf{1}_{R,R}\text{-Ni})_2\text{Pd}$ at 185 °C.

Table S4. Observed GIXRD data of the liquid crystalline phases of $(\mathbf{1}_{R,R}\text{-Ni})_2\text{Pd}$, diffraction angles $2\theta_{\text{obs}}$ (º), Miller indices *h,k,l, d* value d_{obs} (Å), d_{calc} (Å) are *d* values calculated from the lattice parameters of $(\mathbf{1}_{R,R}\text{-Ni})_2\text{Pd}$ at 100 °C, 185 °C, and 204 °C.

Temperature (ºC)	$2\theta_{\text{obs}}$ (º)	*hk*	d_{obs} (Å)	d_{calc} (Å)	$d_{\text{obs}} - d_{\text{calc}}$ (Å)	2D cell parameter
100	2.13	(100)	41.5	–	–	Cr *a* = 48.8 Å
	3.61	(110)	24.4	23.9	0.45	
	4.24	(200)	20.8	20.7	0.06	
	5.62	(210)	15.7	15.7	0.02	
	6.38	(300)	13.8	13.8	−0.03	
	7.56	(220)	11.7	12.0	−0.27	
	9.21		9.59	–		
	24.9		3.58	–		
185	2.21	(10)	40.0	–	–	Col_{h} *a* = 46.6 Å
	3.79	(11)	23.3	21.2	0.22	
	4.41	(21)	20.0	20.0	0.01	
	6.66	(30)	13.3	13.3	0.03	
	8.02	(22)	11.0	11.5	−0.53	
204	2.31	(10)	38.2	–	–	Col_{h} *a* = 44.2 Å
	4.00	(11)	22.1	22.1	0.01	

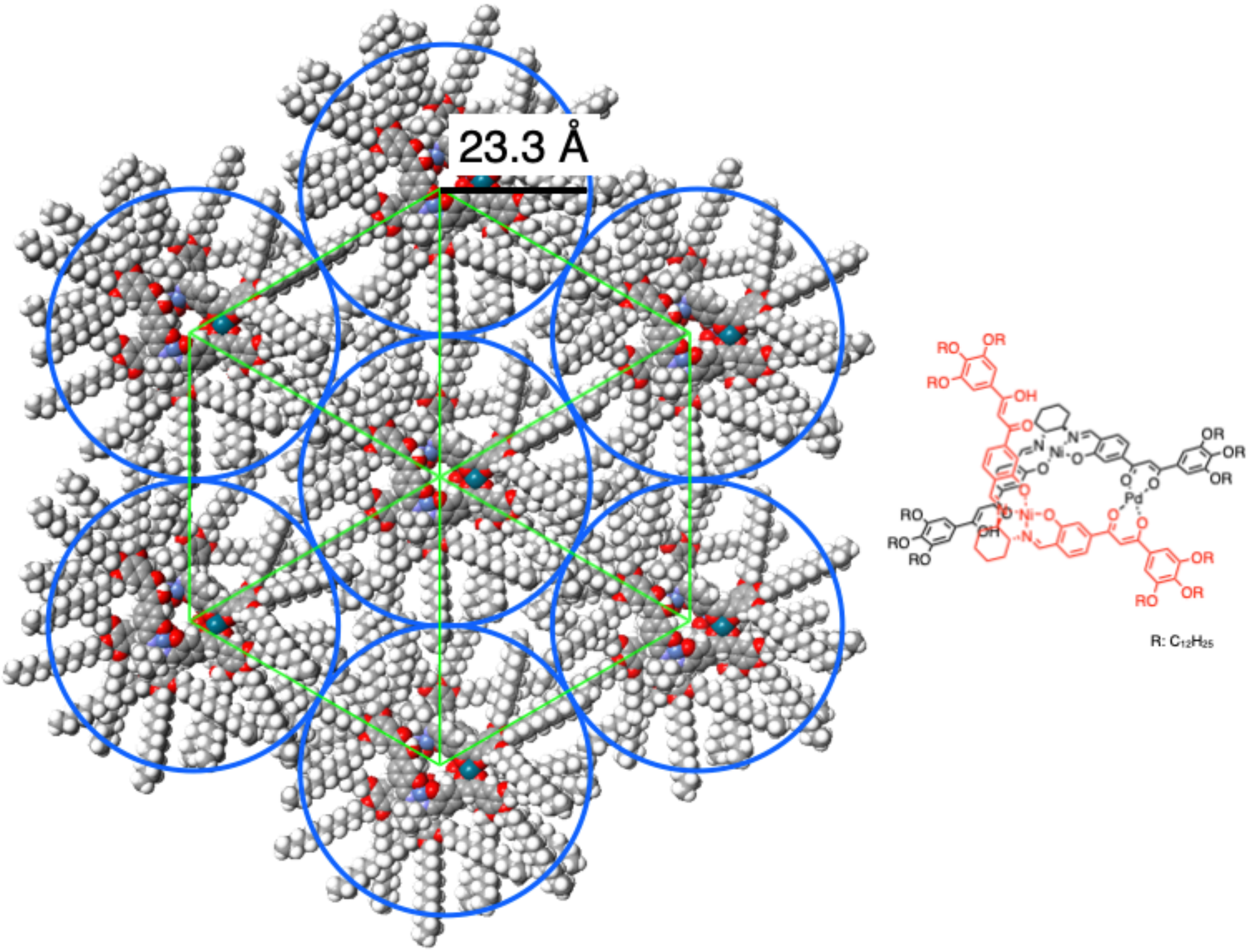

Figure S34. Tentative model of the packing structure of $(\mathbf{1}_{R,R}\text{-Ni})_2$Pd at 185 °C.

8-10. IR spectrum of $(\mathbf{1}_{R,R}\text{-Ni})_2\text{Pd}$

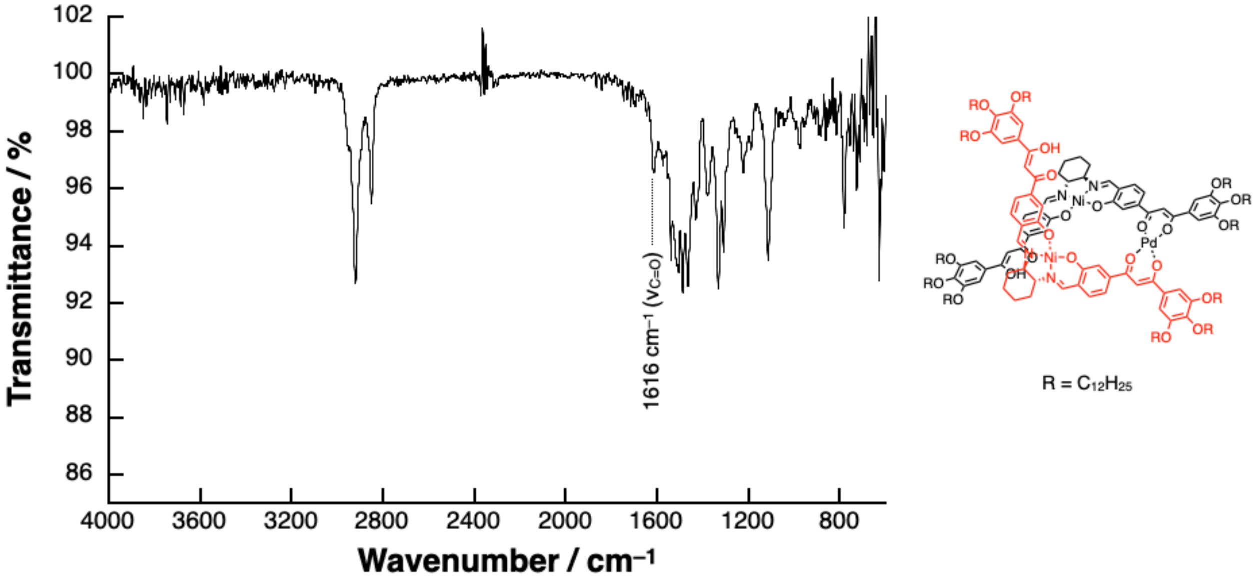

Figure S35. IR spectrum of $(\mathbf{1}_{R,R}\text{-Ni})_2\text{Pd}$ at 22 °C (ATR method).

8-11. Microscopic polarized IR spectrum of $(\mathbf{1}_{R,R}\text{-Ni})_2\text{Pd}$

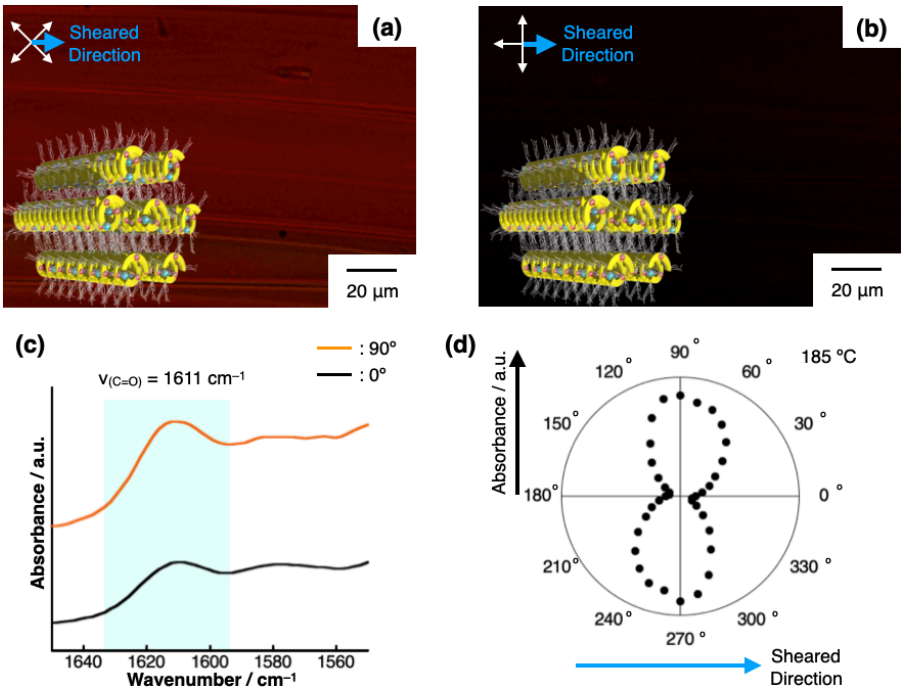

Figure S36. POM images of the sheared sample of $(\mathbf{1}_{R,R}\text{-Ni})_2\text{Pd}$ at 185 °C with the polarizer set to (a) 45° and (b) 0° to the sheared direction. (c) Microscopic IR spectra recorded at 185 °C. The polarized light is set to 90° (orange line) and 0° (black line) to the shearing direction (d) Polar plot of the β-diketonate C=O stretching band of $(\mathbf{1}_{R,R}\text{-Ni})_2\text{Pd}$.

($\mathbf{1}_{R,R}$-Ni)$_2$Pd can be sheared due to the flowable LC properties at 185 °C. As shown in Figure S36, POM image of the sheared sample showed a homogeneous bright birefringence with the sheared direction oriented by 45° to the polarizers. In contrast, when the sheared direction was set parallel to the one of the polarizers, the dark image was observed. These results indicate the columnar assembly of ($\mathbf{1}_{R,R}$-Ni)$_2$Pd could be readily aligned to the sheared direction at the LC phase temperature. In microscopic IR spectra of ($\mathbf{1}_{R,R}$-Ni)$_2$Pd at the LC state, a peak corresponding to the anionic C=O stretching of acetylacetonate moiety appear around at 1611 cm^{-1}. The C=O stretching bond have a maximum when the polarizer is set to 90° with respect to the sheared direction. Relatively large dichroic ratio ($A_{\parallel}/A_{\perp}$) of 1.9 in the absorbance regarding the C=O stretching band was observed. Also, the O–C=C–C stretching band derived from the metal-free β-diketonate moiety of ($\mathbf{1}_{R,R}$-Ni)$_2$Pd showed a dichroic ratio ($A_{\parallel}/A_{\perp}$) of 1.7 in the absorbance. These results clearly illustrate that the planar Pd-bis(diphenyl-β-diketonate) moiety orients perpendicular to the long axis of the columnar assembly.

9. References

(1) E. Campaigne, H. A. Smith, Jr., J. S. Sandhu, C. S. Kim, *J. Heterocyclic. Chem.,* 1983, **20**, 55–59.

(2) M. Peterca, V. Percec, M. R. Iman, P. Leowanawat, K. Morimitsu, P. A. Heiney, *J. Am Chem. Soc.,* 2008, **130**, 14840–14852.

(3) V. Bertolasi, L. Pretto, G. Gilli, P. Gillli. *Acta Crystallogr., Sect. B. Struct. Sci.,* 2006, **62**, 850–863.

(4) D. Steinborn, S. Schwieger, *Chem. Eur. J.,* 2007, **13**, 9668–9678.

(5) S. Grimme, J. Antony, S. Ehrlich, H. Krieg, *J. Chem. Phys.*, 2010, **132**, 154104.

(6) Gaussian 16, Revision B.01, M. J. Frisch, G. W. Trucks, H. B. Schlegel, G. E. Scuseria, M. A. Robb, J. R. Cheeseman, G. Scalmani, V. Barone, G. A. Petersson, H. Nakatsuji, X. Li, M. Caricato, A. V. Marenich, J. Bloino, B. G. Janesko, R. Gomperts, B. Mennucci, H. P. Hratchian, J. V. Ortiz, A. F. Izmaylov, J. L. Sonnenberg, D. Williams-Young, F. Ding, F. Lipparini, F. Egidi, J. Goings, B. Peng, A. Petrone, T. Henderson, D. Ranasinghe, V. G. Zakrzewski, J. Gao, N. Rega, G. Zheng, W. Liang, M. Hada, M. Ehara, K. Toyota, R. Fukuda, J. Hasegawa, M. Ishida, T. Nakajima, Y. Honda, O. Kitao, H. Nakai, T. Vreven, K. Throssell, J. A. Montgomery, Jr., J. E. Peralta, F. Ogliaro, M. J. Bearpark, J. J. Heyd, E. N. Brothers, K. N. Kudin, V. N. Staroverov, T. A. Keith, R. Kobayashi, J. Normand, K. Raghavachari, A. P. Rendell, J. C. Burant, S. S. Iyengar, J. Tomasi, M. Cossi, J. M. Millam, M. Klene, C. Adamo, R. Cammi, J. W. Ochterski, R. L. Martin, K. Morokuma, O. Farkas, J. B. Foresman, and D. J. Fox, Gaussian, Inc., Wallingford CT, 2016.